

**PROCESSING, MICROSTRUCTURES AND PROPERTIES OF ULTRA-HIGH
STRENGTH, LOW CARBON AND V-BEARING DUAL-PHASE STEELS PRODUCED
ON CONTINUOUS GALVANIZING LINES**

by

Yingjie Wu

B. Eng. in Welding Technology and Engineering, Nanchang Hangkong University, 2014

Submitted to the Graduate Faculty of
Swanson School of Engineering in partial fulfillment
of the requirements for the degree of
Master of Science

University of Pittsburgh

2017

UNIVERSITY OF PITTSBURGH
SWANSON SCHOOL OF ENGINEERING

This thesis was presented

by

Yingjie Wu

It was defended on

July 11, 2017

and approved by

Ian Nettleship, Ph.D., Associate Professor, Department of Mechanical Engineering and
Materials Science

Patrick Smolinski, Ph.D., Associate Professor, Department of Mechanical Engineering and
Materials Science

John F. Oyler, Ph.D., Adjunct Associate Professor, Department of Civil and Environment
Engineering

Thesis Advisor: Anthony J. DeArdo, Ph.D., Professor, Department of Mechanical Engineering
and Materials Science

Copyright © by Yingjie Wu

2017

**PROCESSING, MICROSTRUCTURES AND PROPERTIES OF ULTRA-HIGH
STRENGTH, LOW CARBON AND V-BEARING DUAL-PHASE STEELS PRODUCED
ON CONTINUOUS GALVANIZING LINES**

Yingjie Wu, M.S.

University of Pittsburgh, 2017

One of the most popular elements in weight reduction programs in the automotive industry is high strength zinc coated dual-phase steel produced on continuous hot dipped galvanizing lines. The high strength is needed for mass reduction, while the protective zinc coating is needed to prevent corrosion of the thin gage cold rolled steel. The present study was aimed to explore an optimized way to produce such dual-phase steels with ultra-high tensile strength ($UTS > 1280\text{MPa}$), good global ductility ($TE > 18\%$), excellent local ductility (sheared-edge ductility, $HER > 40\%$) and products of $UTS \times TE > 22000\text{ MPa} \times \%$, conforming to data of AHSS Generation III steel. A steel of this kind is referred to as a third-generation advanced high strength steel. By altering chemical compositions (0.15wt.% carbon), pre-annealing conditions (different hot band coiling temperatures and cold reductions), annealing conditions (different intercritical annealing temperatures) and annealing paths (standard galvanizing or supercool processing), this study set out to investigate the effects of these factors on the microstructures and mechanical properties of dual-phase steels. Results showed that the stored energy of cold rolled steel with 0.15wt.% carbon was much higher than that of carbon containing 0.1wt.% carbon, generating numerous lattice defects during deformation and providing more driving force for formation of austenite and

recrystallization of ferrite during the intercritical anneal. In addition, it was found that the volume fraction of martensite increased with the combination of low coiling temperature, high cold reduction, and high annealing temperature, thereby increasing the tensile strength. Furthermore, the microstructural analysis and tensile testing results and showed that the tensile strength of dual-phase steel with 0.15Wt.% carbon, combined with the ultrafine microstructures (average ferrite grain sizes reached 1-2 μ m) could approach 1300MPa without loss of ductility and with hole expansion ratios, in some cases, reaching 35%. Since the relative hardness of the hard martensite and soft ferrite is important in controlling sheared-edge ductility, the nanohardness results of these phases were measured. It was revealed that the martensite hardness decreased with increasing volume fraction, at a given carbon content, indicating the tensile strength was independent of the martensite hardness. Other mechanical properties, such as yield strength, YS/UTS ratio, hardness and work hardening behavior, of dual-phase steels controlled by the factors mentioned above were correlated to the microstructural features. The hypothesis that the bulk carbon content would be a major factor in controlling the strength of these steels was vindicated by the results of this study.

TABLE OF CONTENTS

ACKNOWLEDGEMENT	XIV
1.0 INTRODUCTION.....	1
2.0 KNOWLEDGE BACKGROUND	3
2.1 PRODUCTION ROUTES FOR DUAL- PHASE STEELS	3
2.1.1 Continuous annealing.....	3
2.1.2 As-hot-rolled.....	5
2.1.3 Batch annealing.....	5
2.2 ALLOYING ELEMENTS.....	6
2.2.1 Manganese	6
2.2.2 Silicon.....	7
2.2.3 Chromium and molybdenum.....	8
2.2.4 Vanadium.....	9
2.3 MECHANICAL PROPERTIES OF DUAL PHASE STEELS	10
2.3.1 Yield and tensile strengths	12
2.3.2 Work hardening behavior.....	14
2.4 STRENGTHENING MECHANISMS	16
2.4.1 Grain-size strengthening	16
2.4.2 Precipitation hardening.....	17

2.5	FORMATION OF AUSTENITE.....	20
3.0	STATEMENT OF OBJECTIVE	22
4.0	EXPERIMENTAL PROCEDURES	24
4.1	CHEMICAL COMPOSITIONS OF MATERIALS.....	24
4.2	THERMOMECHANICAL PROCESS	24
4.3	EQUIPMENT AND FACILITIES	32
4.3.1	Optical microscopy	32
4.3.2	Scanning electron microscopy and electron backscatter diffraction	33
4.3.3	Tensile test	34
4.3.4	Vickers hardness test and nano hardness test.....	35
4.3.5	Hole expansion ratio test	37
4.3.6	Vibrating sample magnetometer	38
5.0	RESULTS	40
5.1	RESULTS OF COLD ROLLED STEELS	40
5.2	RESULTS OF ANNEALED STEELS	44
5.2.1	Mechanical Properties	44
5.2.2	Microstructures.....	60
5.2.3	Nanohardness of ferrite and martensite	70
5.2.4	Measurement of retained austenite	74
6.0	DISCUSSION	78
7.0	CONCLUSIONS	82
8.0	FUTURE WORK	84
	BIBLIOGRAPHY.....	85

LIST OF TABLES

Table 4.1 Chemical compositions of materials (w.t%).....	24
Table 4.2 Defining optimum annealing temperature	26
Table 4.3 Critical temperatures of annealed dual phase steels, as the intercritical temperatures chosen 770°C and 750°C, estimated by JmatPro.....	30
Table 4.4 Designation of tested samples based on different coiling temperatures (CT), cold reduction (CR), and intercritical annealing temperatures (IAT)	31
Table 5.1 Designation of cold rolled steels based on different coiling temperatures (CT) and cold reductions (CR)	40
Table 5.2 Vickers hardness (300gf) of cold rolled steels with different coiling temperatures (CT) and cold reductions (CR).....	41
Table 5.3 Stored Energy (J/cm ³) in Cold Rolled Steels Before Annealing.....	43
Table 5.4 Mechanical properties (UTS, YS, TE, YS/UTS, UTS×TE) of the annealed steels with standard galvanizing (F1).....	53
Table 5.5 Mechanical properties (UTS, YS, TE, YS/UTS, UTS×TE) of the annealed steels with supercool processing (G1).....	53
Table 5.6 RA, HER, UTS, TE and UTS×TE of dual phase steels.....	55
Table 5.7 RA, HER (predicted from RA data), UTS, of dual phase steels.....	55
Table 5.8 Work hardening behavior n ₁ (0.2%-0.5% engineering strain), n ₂ (4%-6% engineering strain) and uniform elongation (UE) of annealed steels with standard galvanizing (F1) and supercool processing (G1)	58
Table 5.9 Ferrite grain sizes (d _F), volume fraction of martensite (V _m) and retained austenite(V _{γ'}) of steels annealed by standard galvanizing (F1).....	68
Table 5.10 Ferrite grain sizes (d _F), volume fraction of martensite (V _m), tempered martensite (V _{TM}) and retained austenite(V _{γ'}) of steels annealed by supercool processing (G1). 68	68

Table 5.11 Nanohardness of ferrite and martensite of dual-phase steels annealed by standard galvanizing (F1)..... 73

Table 5.12 Volume fraction of retained austenite ($V_{\gamma'}$) of dual-phase steels annealed by standard galvanizing (F1) and supercool processing (G1)..... 75

LIST OF FIGURES

Figure 2.1 Relationship between the critical cooling rates and alloying elements [23]	7
Figure 2.2 Effect of cooling rate on yield and tensile strengths, YS/UTS, yield point elongation and total elongation in Cr-bearing steels [23]	9
Figure 2.3 Solubility products, in atomic per cent, of carbides and nitrides in austenite as function of temperature [34]	10
Figure 2.4 The relationship between the strengths and percent martensite as well as the distribution of strengths of the fine-grained and the coarse-grained for the Fe-Mn-C alloys [29]....	11
Figure 2.5 The relationship between uniform elongation and tensile strength [29]	12
Figure 2.6 Dislocations bypass the particles [58]	17
Figure 2.7 Dislocations shear the particles [58].....	17
Figure 2.8 Balance of forces acting during particle resistance to dislocation movement [58].....	18
Figure 4.1 Volume fractions of martensite at different annealing temperatures	27
Figure 4.2. Schematic of thermomechanical process.....	30
Figure 4.3 CCT of intercritical austenite during cooling, assuming the equilibrium at AC3 (770°C or 750°C)	31
Figure 4.4 Sony digital camera attached to a Nikon Microscope	33
Figure 4.5 FEI Apreo SEM.....	34
Figure 4.6 Schematic of sheet tensile test samples [68]	35
Figure 4.7 Hysitron TriboIndenter	36
Figure 4.8 The schematic of hole expansion test procedure [69]	37
Figure 4.9 LakeShore vibrating sample magnetometer	39

Figure 5.1 OM images of microstructures of cold rolled steels, etched by 2% Nital, a) 5M (CT=500°C, CR=58%), b) 6M (CT=650°C, CR=58%), c) 5N (CT=500°C, CR=72%), d) 6N (CT=650°C, CR=72%)	41
Figure 5.2 Stored energy of cold rolled steels, a) 5M (CT=500°C, CR=58%) IPF (with HAGB), b) 5M SE=5.01J/cm ³ , c) 6M (CT=650°C, CR=58) IPF (with HAGB), d) 5M SE=5.13J/cm ³ , e) 5N (CT=500°C, CR=58%) IPF (with HAGB), f) 5N SE=5.72J/cm ³ , g) 6N (CT=650°C, CR=72%) IPF (with HAGB), h) 6N SE=5.60J/cm ³	42
Figure 5.3 Engineering stress-strain curve of annealed steels with cold reduction of 58% (left) and cold reduction of 72% (right) annealed by standard galvanizing (F1)	45
Figure 5.4 Engineering stress-strain curve of annealed steels with cold reduction of 58% (left) and cold reduction of 72% (right) annealed by supercool processing (G1)	45
Figure 5.5 Ultimate tensile strength (UTS) of dual phase steels annealed by standard galvanizing (F1) and supercool processing (G1), in terms of each of annealing process, 5 represents CT=500°C, 6 means CT=650°C, M indicates CR=58%, N is CR=72%, X=7 IAT=750°C and X=8 IAT=770°C	48
Figure 5.6 Yield strength (YS) of dual phase steels annealed by standard galvanizing (F1) and supercool processing (G1), in terms of each of annealing process, 5 represents CT=500°C, 6 means CT=650°C, M indicates CR=58%, N is CR=72%, X=7 IAT=750°C and X=8 IAT=770°C	49
Figure 5.7 YS/UTS of dual phase steels annealed by standard galvanizing (F1) and supercool processing (G1), in terms of each of annealing process, 5 represents CT=500°C, 6 means CT=650°C, M indicates CR=58%, N is CR=72%, X=7 IAT=750°C and X=8 IAT=770°C	50
Figure 5.8 Total elongation (TE) of dual phase steels annealed by standard galvanizing (F1) and supercool processing (G1), in terms of each of annealing process, 5 represents CT=500°C, 6 means CT=650°C, M indicates CR=58%, N is CR=72%, X=7 IAT=750°C and X=8 IAT=770°C	51
Figure 5.9 The relationship between total elongation and tensile strength of dual phase steels annealed by standard galvanizing (F1) and supercool processing (G1), blue solid line shows the minimum product of TE×UTS for DP steels (10K), red dashed line represents the minimum product of TE×UTS for TRIP steels (18K), and green dotted line indicates the minimum product of TE×UTS for Generation III steels (22K).....	52
Figure 5.10 The relationship among hole expansion ratios (HER), tensile strength (UTS) and reductions in area (RA). (a) HER (measured) vs RA; (b) HER (predicted from RA) vs UTS.....	56
Figure 5.11 a) n values at 4%-6% engineering strain of steels annealed by standard galvanizing (F1); b) n values at 4%-6% engineering strain of steels annealed by supercool processing (G1); c) the relationship between uniform elongations (10 mm gage length) and n values,	

and the fitting curve of these data is a positive straight line, of which the linear equation is $UE=4.52+31.26 \times n$, with $R^2=0.72$ 59

- Figure 5.12 SEM microstructures of annealed steels with different intercritical annealing temperatures (IAT), a) 5N7J (CT=500°C, CR=72%, AT=750°C, IHT=15s), F1(Standard Galvanizing), b) 5N8J (CT=500°C, CR=72%, AT=770°C, IHT=15s), F1(Standard Galvanizing) 62
- Figure 5.13 SEM microstructures of annealed steels with different intercritical annealing temperatures (IAT), a) 5M7J (CT=500°C, CR=58%, AT=750°C, IHT=15s), F1(Standard Galvanizing), b) 5M8J (CT=500°C, CR=58%, AT=770°C, IHT=15s), F1(Standard Galvanizing) 62
- Figure 5.14 SEM microstructures of annealed steels with different isothermal holding time (IHT) at zinc pot temperature, a) 5N8J (CT=500°C, CR=72%, AT=770°C, IHT=15s), F1(Standard Galvanizing), b) 5N8K (CT=500°C, CR=72%, AT=770°C, IHT=30s), F1(Standard Galvanizing) 63
- Figure 5.15 SEM microstructures of annealed steels with different isothermal holding time (IHT) at zinc pot temperature, a) 5M8J (CT=500°C, CR=58%, AT=770°C, IHT=15s), F1(Standard Galvanizing), b) 5M8K (CT=500°C, CR=58%, AT=770°C, IHT=30s), F1(Standard Galvanizing) 63
- Figure 5.16 SEM microstructures of annealed steels with different coiling temperatures, a) 5N7J (CT=500°C, CR=72%, AT=750°C, IHT=15s), F1(Standard Galvanizing), b) 6N7J (CT=650°C, CR=72%, AT=750°C, IHT=15s), F1(Standard Galvanizing) 64
- Figure 5.17 SEM microstructures of annealed steels with different cold reduction, a) 5N8J (CT=500°C, CR=72%, AT=770°C, IHT=15s), F1(Standard Galvanizing), b) 5M8J (CT=500°C, CR=58%, AT=770°C, IHT=15s), F1(Standard Galvanizing) 64
- Figure 5.18 SEM microstructures of annealed steels with different annealing paths, a) 5N8J (CT=500°C, CR=72%, AT=770°C, IHT=15s), F1(Standard Galvanizing), b) 5N8J (CT=500°C, CR=72%, AT=770°C, IHT=15s), G1(Supercool processing) 65
- Figure 5.19 SEM microstructures of annealed steels with different annealing paths, a) 5M8J (CT=500°C, CR=58%, AT=770°C, IHT=15s), F1(Standard Galvanizing), b) 5M8J (CT=500°C, CR=58%, AT=770°C, IHT=15s), G1(Supercool processing) 65
- Figure 5.20 The relationship between stress and volume fraction of martensite of steels annealed by standard galvanizing (F1) in this research, the upper solid line illustrates the relationship between UTS and V and the lower solid line represents YS and Vm have a linear relation, proposed by Davies. 69
- Figure 5.21 Distribution of ferrite grain sizes of 6M7K (CR=58%) and 6N7K (CR=72%) with standard galvanizing (F1) 69

Figure 5.22 SEM images of nanoindenters, a) 5M7J (CT=500°C, CR=58%, IAT=750°C), and b) 5M8J (CT=500°C, CR=58%, IAT=770°C)	72
Figure 5.23 SEM images of nanoindenters a) 6M7J (CT=650°C, CR=58%, IAT=750°C), and b) 6M8J (CT=650°C, CR=58%, IAT=770°C)	72
Figure 5.24 SEM images of nanoindenters a) 5N7J (CT=500°C, CR=72%, IAT=750°C), and b) 5N8J (CT=500°C, CR=72%, IAT=770°C).....	73
Figure 5.25 SEM images of nanoindenters a) 6N7J (CT=650°C, CR=72%, IAT=750°C), and b) 6N8J (CT=650°C, CR=72%, IAT=770°C).....	73
Figure 5.26 The relationship between nanohardness of martensite (NHNm) and volume fraction of martensite (Vm) of steels annealed by standard galvanizing (F1).	74
Figure 5.27 The relationship between hole expansion ratio and nanohardness of difference of martensite and ferrite	74
Figure 5.28 The Moment/Mass vs Field of dual-phase steel 5M8K, G1	75
Figure 5.29 Volume fraction of retained austenite vs annealing temperate of dual-phase steels annealed by standard galvanizing (F1) and supercool processing (G1).....	77
Figure 5.30 The relationship between HER (predicted from RA data) or RA and volume fraction of retained austenite ($V\gamma'$). a) HER (predicted) vs $V\gamma'$, with the fitting curve of $HER=5.84\times V\gamma'+11.38$, $R^2=0.59$, b) $RA=4.71\times V\gamma'+18.05$, $R^2=0.57$	77

ACKNOWLEDGEMENT

I would like to convey my gratefulness to many people, because without their constant advice, forbearance and encouragement, I would never complete this thesis.

First and foremost, I would like to extend my gratitude to my advisor, Dr. Anthony J. DeArdo. His profound knowledge and extensive experience on physical metallurgy is always the strongest support and guidance for my study. And then I want to thank the other committee members, Professors Nettleship, Smolinski and Oyler for reviewing my thesis, attending my thesis defense and providing precious comments and suggestions.

Secondly, I would like to give a special thank you to Dr. Hua who helped me very much with sample preparation, mechanical testing and research, and etching methods selection. Subsequently, I wish to thank Qiongshu Wang for her continuous encouragement on my study and daily life. And I also need to thank other BAMPRI members, Bing Ma, Yu Gong, Petch Janbanjong, Junyu Duan, Xinchu Feng and Aaron Stein. No matter what kind of difficulties I encountered, they were willing to help me without any hesitation. Our friendship is the most valuable asset in my life.

In particular, I wish to extend my thanks to Dr. Goldman who helped me to improve my English speaking and writing skills, and he was always patient to correct all the mistakes I make.

Last but not least, I want to thank my parents, because without their financial support and mental encouragement, I would never finish my M.S. program in University of Pittsburgh.

1.0 INTRODUCTION

Dual-phase steels are characterized by a microstructure comprising of mainly of ferrite and martensite [1], but sometimes with a third phase, such as bainite, tempered martensite and retained austenite , leading to high tensile strength, continuous yielding, a low YS/UTS ratio, a high strain hardening rate and good ductility. These unique properties, as well as low alloy and continuous galvanizing line production costs, enable dual-phase steel to become the highly competitive materials in the automobile industry.

Today, DP 590 (UTS=590MPa), DP 780 (UTS=780MPa) and DP 980 (UTS=980 MPa) are commercial products, while DP 1180 (UTS=1180MPa) and DP1380 (UTS=1380 MPa) are still being investigated [1]. The difference in the mechanical properties of these steels is mainly attributed to the final microstructures. The tensile strength is linearly related to the volume fraction of martensite [2], which is transformed from intercritical austenite during cooling. Thus, understanding the formation of austenite during intercritical annealing is very important [1] and it is controlled by many obvious factors, such as alloying elements, reheating rates, intercritical annealing temperature, cooling rates from the annealing temperature to the zinc pot temperature and residency time in the zinc pot. However, this and other recent studies [3] [4] have shown secondary pre-annealing effects such as hot band coiling temperature and cold reduction can also greatly influence the amount of austenite formed during the anneal. Therefore, a good combination of coiling temperature and cold reduction can help ensure that a large amount of austenite can be

obtained during intercritical annealing in the short time available [5]. It has been found that the stored energy of the cold band is a good indicator to evaluate the ability to form large amounts of austenite during the anneal. The higher the stored energy, the larger the amount of new austenite will be formed. During intercritical annealing, a high annealing temperature will ensure more austenite to form, from the level rule, and after cooling, a large amount of martensite is attained to increase the tensile strength. The microstructures and mechanical properties also can be controlled by chemical compositions, such as carbon.

The properties of dual-phase steels containing 0.10wt% carbon were investigated by many researcher, but the benefit of changing carbon content from 0.10wt% to 0.15wt% is obvious. At the same intercritical annealing temperature, the dual-phase steels with 0.15wt% carbon can have more volume fraction of martensite, compared with 0.10wt% carbon, thereby increasing the hardness and tensile strength. The dual-phase steel with 0.15wt% carbon and 50% martensite have a good combination of high strength and good ductility [6], which helps to achieve the purpose of this study.

In terms of annealing path, apart from standard galvanizing, a new supercool processing was also used in this study. This new supercool processing is similar to quenching and partitioning process (Q&P). The dual-phase steels annealed by supercool processing can yield a good balance of high strength and good ductility. In the beginning of the supercool process, like quenching step, the intercritically annealed austenite were fast cooled from anneal temperature to supercool temperature (between M_s and M_f temperature) to from a controlled volume fraction of martensite [7]. After quenching, the steels were up quenched to zinc pot temperature (between B_s and M_s temperature), which is similar to portioning process.

2.0 KNOWLEDGE BACKGROUND

2.1 PRODUCTION ROUTES FOR DUAL- PHASE STEELS

Producing technologies of dual phase steels comprise three procedures: as-hot-rolled, batch annealing, and continuous annealing, with continuous annealing the most widely used. This is because of the higher production rates, better uniformity of properties, and the possibility of using low alloying elements [8].

2.1.1 Continuous annealing

The cold rolled DP steels typically use continuous annealing. During intercritical annealing, the steels are heated up between the A_1 and A_3 critical temperatures and soaked for a short time to anneal the cold rolled ferrite and form austenite. These austenite-ferrite mixtures are then accelerated cooled to the zinc pot temperature of approximately 460°C [9] [10].

During continuous annealing, the formation of final microstructures of dual phase steels consists of several steps; formation of austenite during intercritical annealing, transformation of austenite after intercritical annealing and changes in ferrite during intercritical annealing [9] [11] [12] [13].

According to the level rule, higher intercritical annealing temperatures increase the amount of austenite and lead to a lower amount of carbon in the austenite, thereby decreasing the hardenability of austenite [14]. At low intercritical annealing temperatures, where the amount of austenite is low, the carbon content of the austenite is high, resulting in high hardenability of the intercritically formed austenite [15] [16].

In addition to intercritical annealing temperatures, the cooling rates from the annealing temperature to the zinc pot temperature can influence the final microstructures of dual-phase steels [1]. Since the zinc pot temperature of 460°C is higher than the M_s but lower than the B_s of the intercritically formed austenite, high cooling rates will suppress the formation of new ferrite and bainite during cooling [17]. However, at the lower cooling rates, the portion of the intercritically formed austenite would transform into ferrite and ferrite-carbide mixtures (pearlite or bainite). Also, at the lower cooling rate, where cementite can precipitate in the ferrite, this would contribute to low carbon contents in ferrite; the epitaxial ferrite formed at slower cooling rates will maintain equilibrium with the austenite, following the Ac_3 phase boundary line, consequently lowering the carbon content in ferrite [18]. The mechanical properties of dual-phase steels are affected by cooling rates after intercritical annealing. At the lower cooling temperature, the product of ultimate tensile strength \times total elongation ($UTS \times TE$, $\text{MPa} \times \%$) increases remarkably; however, the yield strength to tensile strength ratio (YS/UTS) can be maintained at a low level at lower cooling temperature, such as $10^{\circ}\text{C} / \text{s}$ [19].

2.1.2 As-hot-rolled

In terms of the as-hot-rolled method, the steels are heated above A_3 critical temperature and held for a relatively long time, followed by several rolling passes. The final pass of reduction is done with a low finish rolling temperature at or about A_3 critical temperature. Subsequently, the samples underwent oil quenching or cooling down to coiling temperatures and furnace cooling [19].

Finish rolling temperatures, coiling temperatures and cooling rates after rolling influence the mechanical properties and final microstructures of dual-phase steels. At a higher finish rolling temperature, the final microstructures contain coarse-grained phase, like acicular ferrite; while, the lower coiling temperature contributes to more deformed and rather coarse-grained ferrite and a small amount of martensite in final microstructures. Moreover, the increased coiling temperature improves the yield strength and decreases the ultimate tensile strength, thereby improving the yield strength to ultimate tensile strength ratio (YS/UTS). This trend is attributed to the auto-tempering of martensite and the carbide precipitates in ferrite matrix as the coiling temperature is increased.

2.1.3 Batch annealing

For batch annealing, the heat treatment is similar to continuous annealing; its soaking time is much longer and heating/cooling rates are much slower. This annealing process with slower cooling rates makes it possible for the use of the steels with high level alloying elements and high hardenability [8].

2.2 ALLOYING ELEMENTS

The alloying elements, such as manganese, silicon, chromium, molybdenum, and vanadium used in dual-phase steels can affect grain refinement, hardenability and the formation and morphology of particles. Besides, these alloying elements can influence the tensile strength by solid solution strengthening and precipitation hardening mechanisms, especially the ferrite.

2.2.1 Manganese

Manganese broadens the temperature range for stable austenite and, if added in sufficiently high concentration, the transformation temperatures A_{C1} and A_{C3} decrease and the TTT diagram shifts to the longer time, thus increasing the possibility of forming the ferrite-martensite mixtures at a relatively low cooling rate [20] [21] [22]. Besides, the addition of manganese refines the cementite and reduces the grain sizes, leading to good ductility. Furthermore, the influence of manganese segregation is to form microbands [21], and the austenite is located in the Mn-rich regions; while deformed and recrystallized ferrite develop in the Mn-poor area.

Alloying elements can influence the critical cooling rates of the intercritically formed austenite cooled from the annealing temperature in dual-phase steels. Increasing the alloying elements content decreases the logarithm of the critical cooling rates [23], shown in Figure 2.1. The amount of different alloying elements can be converted into Mn equivalent content (Mn_{eq}^0), which can be obtained by Equation (2-1). The relationship between the critical cooling rate (CR^0) and Mn content (Mn_{eq}^0) can be attained by equation (2-2).

$$Mn_{eq}^0 = Mn(\%) + 2.67Mo(\%) + 1.3Cr(\%) \quad (2-1)$$

$$\log CR^0 (\text{°C/s}) = -1.73Mn_{eq}^0 + 3.95 \quad (2-2)$$

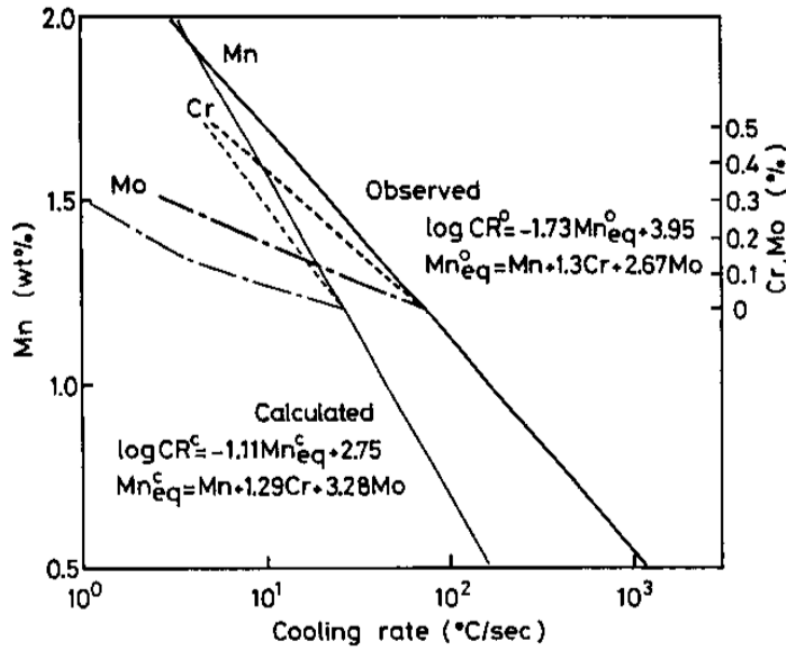


Figure 2.1 Relationship between the critical cooling rates and alloying elements [23]

2.2.2 Silicon

The addition of silicon influences the microstructures and mechanical properties of dual phase steels. Si can promote the formation of ferrite [24] [25] [26], decrease the ferrite grain sizes and change the ferrite shape from irregularity to equiaxed shape. The increasing the amount of Si improves the yield strength, because of hard solid solute strengthening related to the high content of Si and the ferrite grain refinement caused by the addition of Si. The increase in the amount of Si contributes to improving the tensile strength [27], uniform elongation, total elongation, and strain hardening ratio. Therefore, the product of ultimate tensile strength \times total elongation increases with increasing Si content [1].

2.2.3 Chromium and molybdenum

Molybdenum can influence the shape of CCT diagram; it helps to delay the bainite start and bainite finish, to retard pearlite start, and to increase the pearlite finish temperature, thus separating the pearlite-ferrite transformation region and bainite transformation region [28]. Because the dual-phase steels often undergo isothermal holding at zinc pot temperature (460°C), a part of martensite would be replaced by bainite. As a result, the tensile strength would be decreased and the yield strength and ductility could be improved, leading to increasing the YS/UTS ratio and strain hardening ratio. Therefore, when the dual-phase steels are annealed by the galvanizing process, the addition of Mo enables austenite to avoid transformation into bainite or pearlite, ensuring the ferrite-martensite microstructures after annealing.

Figure 2.2 shows the relationship between mechanical properties, such as tensile strength, yield strength, yield strength to tensile strength ratio (YS/UTS), uniform elongation, and total elongation, of Cr-bearing steels and cooling rates. The increasing cooling rate results in increasing tensile strength and decreasing total elongation. As the Cr is increased, both the yield strength and YS/UTS decrease at any cooling rate [23]. Furthermore, the addition of Cr can promote the partitioning of C between austenite and ferrite, thereby decreasing the dissolved carbon content. In addition, the tensile strength of dual-phase steels is dependent on the volume fraction of martensite, which is not only based on carbon content and annealing temperature, but also on the hardenability of austenite. The addition of Cr, Mn and V match the requirement for the hardenability to the cooling rate [29].

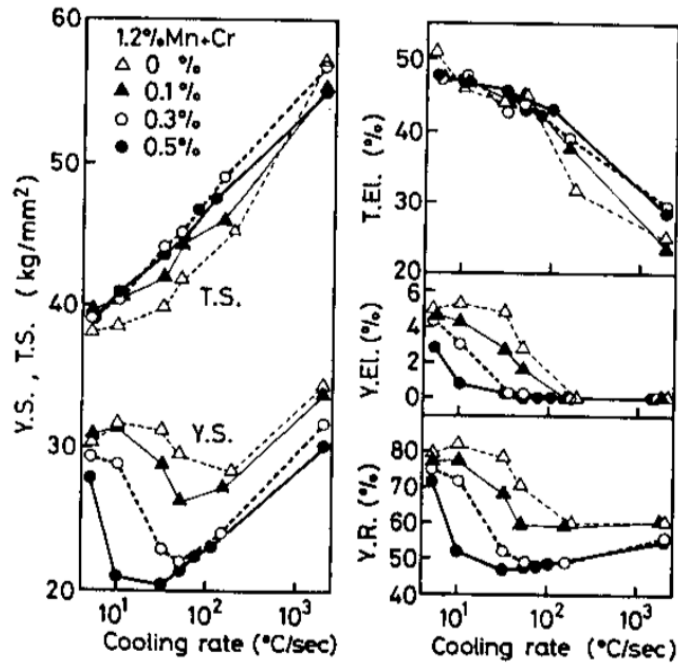


Figure 2.2 Effect of cooling rate on yield and tensile strengths, YS/UTS, yield point elongation and total elongation in Cr-bearing steels [23]

2.2.4 Vanadium

The effects of vanadium used in dual-phase steels are characterized by three factors; the high solubility of vanadium carbonitrides in austenite [30] [31] [32], the low solute drag coefficient of vanadium and the positive interaction of vanadium with nitrogen [30]. The high solubility of vanadium carbonitrides results in remarkable castability with minimum cracking and reduction of the reheating temperature. The excellent precipitation hardening behavior of vanadium carbonitrides is also attributed to the high solubility of vanadium carbonitrides. The low solute drag coefficient contributes to refining austenite grains [33] and minimizing the temperature and the deformation requirements for recrystallization. In addition, because vanadium is the only alloying element that can strengthen steel as nitride precipitates [1], and the solubility of vanadium

carbides is higher than that of vanadium nitrides (Figure 2.3), nitrogen can be used effectively for precipitation hardening at different levels of carbon content.

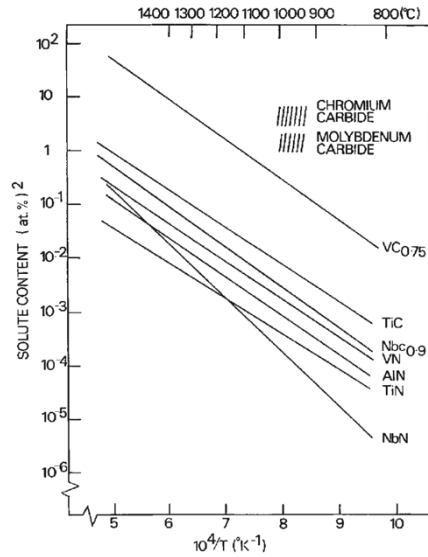


Figure 2.3 Solubility products, in atomic per cent, of carbides and nitrides in austenite as function of temperature [34]

2.3 MECHANICAL PROPERTIES OF DUAL PHASE STEELS

Dual-phase steels are characterized by a microstructure comprising of ferrite, martensite and a third phase, such as bainite, tempered martensite and retained austenite, leading to high tensile strength, continuous yielding, a low YS/UTS ratio, a high strain hardening rate and good ductility [29] [35] [36] [37]. These unique properties are controlled by volume fraction of martensite, ferrite grain sizes, and fine precipitates in the ferrite matrix [1]. [38]

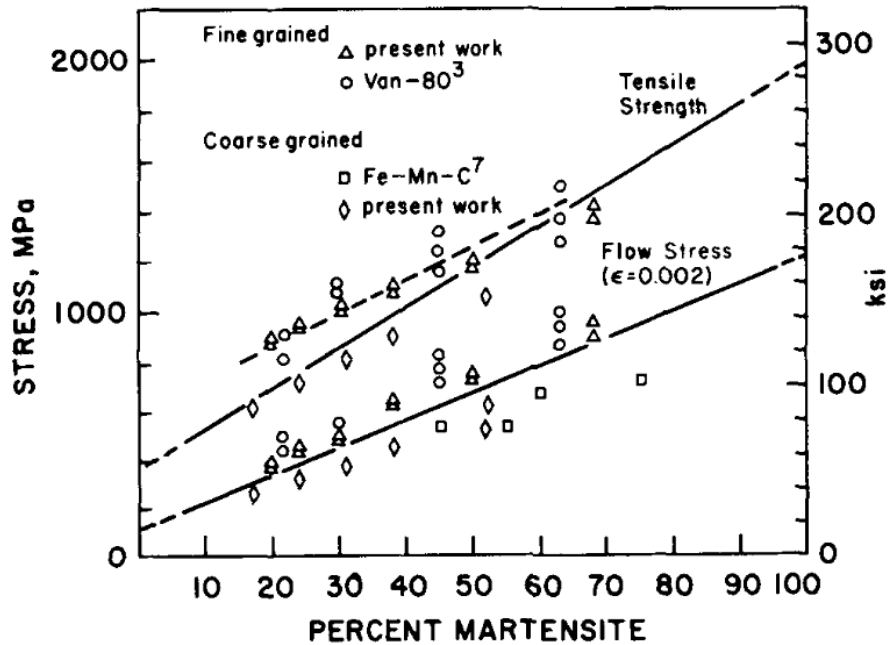


Figure 2.4 The relationship between the strengths and percent martensite as well as the distribution of strengths of the fine-grained and the coarse-grained for the Fe-Mn-C alloys [29]

Figure 2.4 shows the relationship between strengths (yield strength and ultimate tensile strength) and volume fraction of martensite. It is obvious that the strength and martensite content have a positive linear relation; thus, increasing the volume fraction of martensite improves both yield and tensile strengths. Besides, according to Figure 2.4, the strengths of refined grains lie above the yield and tensile strength lines; while the strengths of coarse grains are below the two strength lines, which means the strength of dual-phase steels is also dependent on grain size.

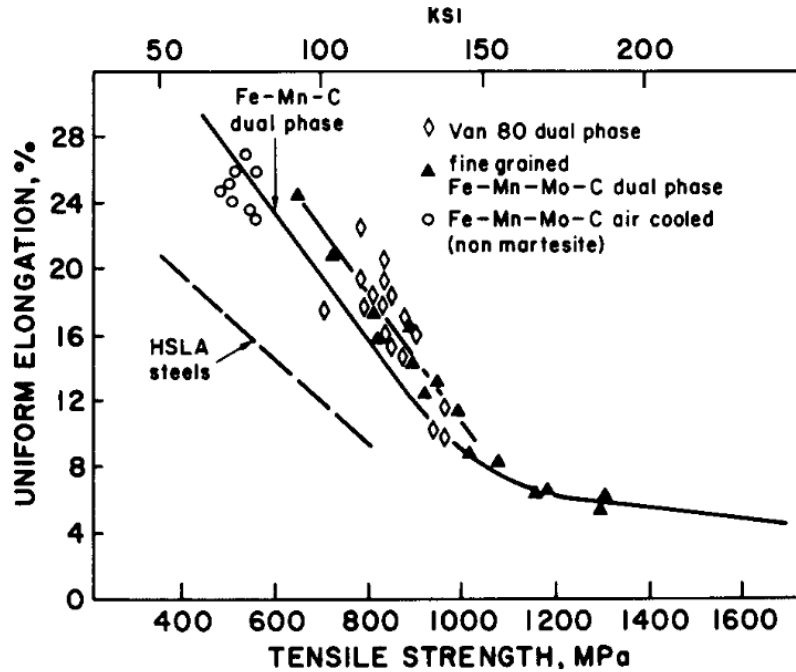


Figure 2.5 The relationship between uniform elongation and tensile strength [29]

Figure 2.5 represents the relationship between uniform elongation and tensile strength. It is obvious that uniform elongation is the function of tensile strength; the increasing tensile strength decreases the uniform elongation [38]. In Figure 2.5, at given tensile strength, the uniform elongation of fine-grained steels is better [38]. Thus, the ductility of dual-phase steels is also controlled by grain sizes.

2.3.1 Yield and tensile strengths

When the volume fraction of martensite or the strength of martensite is increased, it is expected that both yield strength and tensile strength would be improved, following the rule of mixtures. The yield strength and tensile of ferrite-martensite mixed dual-phase steels can be obtained by the Equation (2-3) and (2-4) [9].

$$S_Y^0 = S_{Y,\alpha}^0 \left(\frac{P_\alpha}{100} \right) + S_{Y,m}^0 \left(\frac{P_m}{100} \right) \quad (2-3)$$

$$S_T^0 = S_{T,\alpha}^0 \left(\frac{P_\alpha}{100} \right) + S_{T,m}^0 \left(\frac{P_m}{100} \right) \quad (2-4)$$

where, S_Y^0 is the yield strength of dual-phase steels, $S_{Y,\alpha}^0$ is the yield strength of ferrite, $P_\alpha/100$ is the volume fraction of ferrite, $S_{Y,m}^0$ is the yield strength of martensite, $P_m/100$ is the volume fraction of martensite, S_T^0 is the tensile strength of dual-phase steels, $S_{T,\alpha}^0$ is the tensile strength of ferrite, and $S_{T,m}^0$ is the tensile strength of martensite.

Tumara [39] proposed parameter C,

Because the yield strength for ferrite-martensite mixture did not match the Equation (2-3), except when $P_\alpha = P_m$. If $C < 3$, the yield strength fits the equation; while if $C > 3$, initially the yield strength increased linearly with the increasing of the amount of martensite, and the yield strength increased far away from the trend.

$$C = S_{Y,m}/S_{Y,\alpha} \quad (2-5)$$

Davies [29] found the Equation (2-4) was always correct at any volume fraction of martensite. Speich and Miller [40] put forward the linear relationship between yield and tensile strengths and volume fraction of martensite, which can be expressed in Equation (2-6) and (2-7).

$$S_{Y,m} = S_{Y,\alpha}^0 + \left(\frac{1}{3} S_{Y,m}^0 - S_{Y,\alpha}^0 \right) \left(\frac{P_m}{100} \right) \quad (2-6)$$

$$S_{T,m} = S_{T,\alpha}^0 + \left(\frac{1}{3} S_{T,m}^0 - S_{Y,\alpha}^0 \right) \left(\frac{P_m}{100} \right) \quad (2-7)$$

Leslie and Sober [41] proposed an equation, which illustrated the positive linear relationship between the yield strength of martensite and the carbon content in martensite.

$$S_{Y,m}^0 \text{ (MPa)} = 620 + 258C_m \quad (2-8)$$

where, C_m is the carbon content in martensite and C_m can be expressed in Equation (2-9).

$$C_m = 100(C_o/P_m) \quad (2-9)$$

2.3.2 Work hardening behavior

Work hardening behavior can be expressed by Equation (2-10) [42], which illustrated the relationship between the true stress and true strain.

$$\sigma = K\varepsilon^n \quad (2-10)$$

where, σ is true stress, K is strength coefficient, ε is true strain and n is work hardening exponent.

Taking the logarithm of both sides of Equation (2-10), work hardening exponent n can be obtained by Equation (2-11). This model is Hollomon model.

$$n = \frac{d(\ln \sigma)}{d(\ln \varepsilon)} \quad (2-11)$$

From the $\ln \sigma$ versus $\ln \varepsilon$ curve, n is the slope of the curve. Earlier research [43] [44] [45] exhibited nonlinear variation of $\ln \sigma$ versus $\ln \varepsilon$, which illustrated work hardening of dual phase steels happened in two stages.

Work hardening ratio also can be expressed by Equation (2-12), utilizing the differential Crussard-Jaoul (C-J) analysis [46] [47] [48]. C-J model is the extension of Hollomon model, which includes the yield strength σ_o , allowing better modeling of plastic region [49].

$$\sigma = \sigma_o + K\varepsilon^n \quad (2-12)$$

where, σ_0 and K are materials constant. After logarithmic differentiation with respect to ε , the Equation (2-13) is given.

$$\ln\left(\frac{d\sigma}{d\varepsilon}\right) = \ln(Kn) + (n - 1)\ln\varepsilon \quad (2-13)$$

Compared with other models, differential C-J analysis is more accurate, because n and K can be obtained from $\ln\left(\frac{d\sigma}{d\varepsilon}\right)$ versus $\ln\varepsilon$ curves. The plot of $\ln\left(\frac{d\sigma}{d\varepsilon}\right)$ versus $\ln\varepsilon$ showed that there were three work hardening stages of dual phase steels [50]. These three work hardening stages were attributed to different deformation mechanisms. Stage I consisted of deformation in the ferrite matrix with the high density of dislocation near the ferrite/martensite area [46] [50]. Stage II comprised reduced work hardening ascribed to the deformation of less ferrite with possible transformation from retained austenite to martensite [50]. In terms of stage III, both ferrite and martensite were deformed with attendant cross-slip and dynamic recovery in ferrite [51].

The modified Crussard-Jaoul (C-J) analysis of work hardening behavior was expressed in Equation (2-14).

$$\varepsilon = \varepsilon_0 + c\sigma^m \quad (2-14)$$

where, ε_0 and c are materials constant, m is the inverse of the work hardening exponent. After logarithmic differentiation with respect to σ , the Equation (2-15) was given.

$$\ln\left(\frac{d\sigma}{d\varepsilon}\right) = (1 - m)\ln\sigma - \ln(cm) \quad (2-15)$$

Earlier research revealed two work hardening stages, when the modified C-J analysis was used to investigate the work hardening behavior of dual-phase steels. Two deformation mechanism contributed to these two stages. In stage I, the ferrite with a high density of lattice defects near

the martensite region was deformed. Stage II consisted of the deformation of martensite and hardened ferrite.

2.4 STRENGTHENING MECHANISMS

2.4.1 Grain-size strengthening

The Hall-Petch equation was proposed by Hall [52] and Petch [53], which illustrates the relationship between the yield strength and grain sizes.

$$\sigma_y = \sigma_o + kD^{-1/2} \quad (2-16)$$

where, σ_y is yield strength, σ_o is frictional stress that can move the dislocation, k is the materials constant and D is the grain size. In terms of σ_o , it is related to the undeformed single crystal [54]. While, for the deformed crystal, the Hall-Petch can be rewritten in Equation (2-17), at any strain [55].

$$\sigma(\varepsilon) = \sigma_o(\varepsilon) + k(\varepsilon)D^{-1/2} \quad (2-17)$$

$\sigma_o(\varepsilon)$ is independent on grain sizes and it is the flow stress of the grain interior [55]; while $k(\varepsilon)D^{-1/2}$ depends on grain sizes, and it is the strength attributed to the resistance of the movement of dislocation near the grain boundaries. Equation (2-17) can be expressed by Equation (2-18).

$$\sigma(\varepsilon) = \sigma_o + M\alpha G\sqrt{1.5bS_V\theta} + k(\varepsilon)D^{-1/2} \quad (2-18)$$

where, M is Taylor factor, α is a number, G is shear modulus, b is Burgers vector, S_V is grain boundary area per volume and θ is misorientation angle. At high strain, the low angle grain boundaries (LAGBs) transform into high angle grain boundaries (HAGBs) [56], so the Equation (2-18) can be rewritten by Equation (2-19).

$$\sigma = \sigma_0 + M\alpha G\sqrt{1.5b(S_V\theta)_{LAGB}} + k(\epsilon)D_{HAGB}^{-1/2} \quad (2-19)$$

2.4.2 Precipitation hardening

Finely distributed precipitates have an effective barrier to the movement of dislocations. There are two ways of interpreting the interaction between precipitates and dislocations; dislocations bypass the ‘hard’ particles (shown in Figure 2.6) and dislocations cut through the ‘soft’ particles [57] (shown in Figure 2.7).

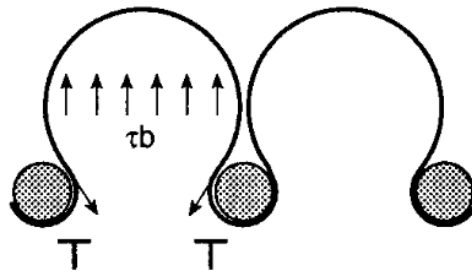


Figure 2.6 Dislocations bypass the particles [58]

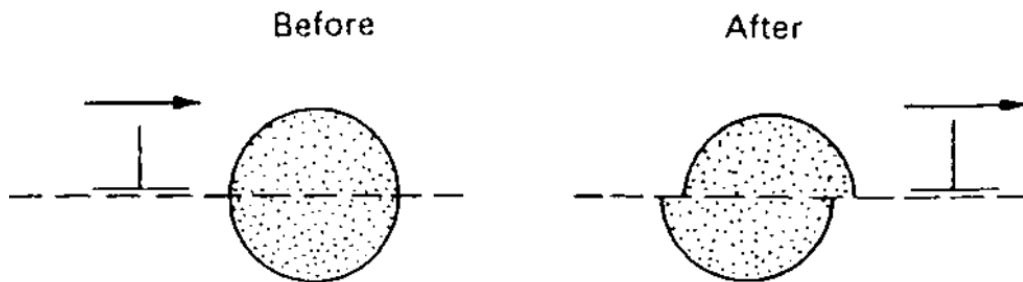


Figure 2.7 Dislocations shear the particles [58]

Figure 2.8 showed the balance of forces between the dislocation line tension T and the resisting force of the particle F . And the relationship of T and F can be expressed by Equation (2-20).

$$F = 2T \sin \theta \quad (2-20)$$

when $\sin \theta = 1$, the resisting force reached the maximum value. And if $F > 2T$, dislocations would bypass the particles. However, if $F < 2T$, dislocations would shear the particles.

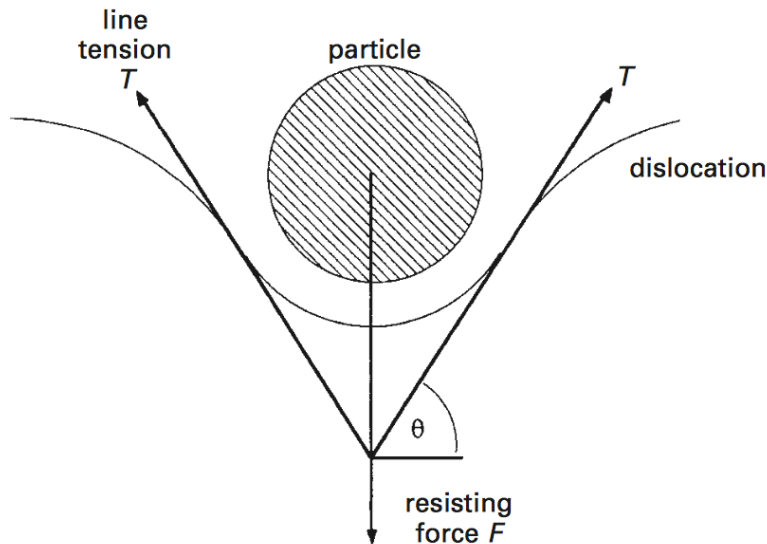


Figure 2.8 Balance of forces acting during particle resistance to dislocation movement [58]

In terms of hard particles, Orowan [59] and Ashby [60] put forward Equation (2-21).

$$\Delta\sigma_y = (0.538Gb f^{1/2}/X)\ln(X/2b) \quad (2-21)$$

where, $\Delta\sigma_y$ is the increase in the yield strength, G is shear modulus of the matrix, b is Burgers vector of dislocations, f is the volume fraction of particles and X is the diameter of particles [61].

From this equation, increasing volume fraction of particles and reducing the diameters of particles resulted in the increase of precipitation strengthening.

In the case of soft particles, there are several effects involved in the precipitation hardening. The deformed particle can lead to an increase in the particle/matrix interfacial energy. The movement of a dislocation through a particle may produce an antiphase boundary with disordering energy or stacking fault energy [58]. So, this effect is called chemical hardening [58]. Mott and Nabarro [62] described coherency strain hardening. The displacements associated with dislocations interact with the coherency strain provide a better strengthening effect than the dislocations alone. The effect of chemical hardening can be expressed by Equation (2-22)

$$\Delta\tau_y = (\gamma^2/b)(4r_s f/\pi T)^{1/2} \quad (2-22)$$

where, τ_y is the increase in the yield stress, γ is the antiphase grain boundary, b is Burgers vector of dislocations, r_s is the average particle radius, f is the volume fraction of particles and T is dislocation line tension. The chemical hardening is related to particle diameters, so the Equation (2-22) can be rewritten by Equation (2-23), in terms of smaller particles.

$$\Delta\tau_y = 4.1G\varepsilon^2(rf/b)^{1/2} \quad (2-23)$$

However, for the larger particles, Equation (2-22) can be rewritten by Equation (2-24).

$$\Delta\tau_y = 0.7Gf^{1/2}\varepsilon^4(b/r)^{3/4} \quad (2-24)$$

Therefore, in the case of smaller particles, the increasing particle diameters improve the strengthening effect; for larger particles, the increasing particle sizes decreases the internal stress.

2.5 FORMATION OF AUSTENITE

The final microstructures of dual phase steels comprise soft ferrite and hard martensite. During intercritical annealing, a ferrite-austenite structure forms, in which the austenite transforms into martensite after rapid cooling [63]. Because the volume fraction of martensite is proportional to the tensile strength of DP steels, the formation of austenite during intercritical annealing is critical, which was investigated by many researchers.

Speich [64] proposed three steps for austenite formation; 1) nucleation of austenite in the pearlite and the grain-boundary cementite particles, followed by rapid growth until the cementite dissolves; 2) slower growth of austenite into ferrite at a rate controlled by the diffusion of carbon in austenite at high temperatures and by manganese diffusion in ferrite at low temperatures; 3) a very slow equilibrium of ferrite and austenite in austenite. Garcia and DeArdo [65] investigated the austenite formation from different initial microstructural conditions, including spheroidized Fe_3C in a recrystallized ferrite matrix, spheroidized Fe_3C in a cold worked ferrite matrix and lamellar ferrite-pearlite structure. They found that austenite formed at ferrite/ferrite grain boundaries for all initial conditions; 1.5 pct. manganese lowered the A_{C1} and A_{C3} critical temperatures, thereby increasing the volume fraction of austenite; the austenite formation rate from cold rolled ferrite was faster than that from recrystallized ferrite and ferrite-pearlite structure. Huang [11] found that the heating rates have effects on the nucleation and growth of austenite for both hot rolled and cold rolled steels. The interaction between austenite formation and ferrite recrystallization was complicated. When the recrystallization of ferrite completed before the formation of austenite, austenite would be distributed randomly in the ferrite matrix.

Mahieu [66] proposed that empirical equation of Johnson-Mehl-Avrami (JMA) associated with Kolmogorov modification (JMAK) can be used to analyze the kinetics of austenite formation.

$$f_{\gamma} = 1 - \exp(-kt^n) \quad (2-25)$$

where, f_{γ} is the volume fraction of austenite, k is the rate constant dependent on annealing temperatures, t is annealing time and n is Avrami's exponent. Asadabad [63] found that increasing annealing time improved the volume fraction of austenite until it reached the maximum value and subsequently austenite volume fraction would not change as time increased; increasing annealing temperature increased the volume fraction of austenite; a new JMA model $f_{\gamma}/f_e = 1 - \exp(-kt^n)$ was put forward to investigate the relationship between volume fraction of austenite and annealing time at different annealing temperatures in the time of intercritical annealing.

3.0 STATEMENT OF OBJECTIVE

This study focuses on the processing, microstructures and properties of ultra-high strength, low carbon and V-bearing dual phase steels on continuous galvanizing lines. The effects of several factors, such as coiling temperatures, cold reduction, intercritical annealing temperatures, and annealing paths, on the properties of dual-phase steels would be investigated. To obtain the structure-property relationship, several characterization methods would be used. In addition, the computer-based simulation would be applied to investigate the phase transformation process.

First, JMatPro thermos-physical and physical properties software will be utilized to study the behavior of new austenite during coiling and cooling and estimate the final microstructures of hot band at different coiling temperatures. In addition, the microstructures, micro hardness and stored energy of received cold rolled steels will be analyzed to investigate the effects of different pre-annealing conditions (hot band coiling temperatures and cold reductions) on microstructures and properties of CR steels.

In the second part, the mechanical properties, including tensile strength, yield strength, YS/UTS ratio, total elongation, $UTS \times TE$, hole expansion ratio and work hardening exponent, of annealed dual phase steels would be investigated so as to reveal the effects of coiling temperatures, cold reduction, annealing temperatures and annealing paths on these unique properties.

In the third section, in order to have a deeper understanding of structure-property relationships of annealed DP steels, the final microstructure characterizations would be conducted with optical microscope, electron scanning microscope and electron backscatter diffraction.

Finally, the nanohardness of annealed dual-phase steels would be measured to study the relationship between the volume fraction of martensite and the nanohardness of martensite and to reveal whether tensile strength can be controlled by martensite hardness.

4.0 EXPERIMENTAL PROCEDURES

4.1 CHEMICAL COMPOSITIONS OF MATERIALS

The chemical compositions obtained of the candidate steels are given in the Table 4.1. Following previous BAMPRI studies, low carbon (0.15 w.t%), high chromium (0.5 w.t%) and molybdenum (0.3 w.t%) and addition of vanadium (0.06 w.t%) are chosen in this study.

Table 4.1 Chemical compositions of materials (w.t%)

Elements	C	Mn	P	S	Si	Cr	Mo	V	Ti	Al	N	Nb
	0.15	1.8	0.01	0.003	0.4	0.5	0.3	0.06	0.005	0.025	0.006	0.005

4.2 THERMOMECHANICAL PROCESS

The whole thermomechanical process is represented in Figure 4.1. In the rough rolling section, the ingots were heated to 1250°C and then rough rolled on a pilot scale hot rolling to the thickness of 25 mm (1 inch), followed by cooling down to room temperature. Furthermore, the steels were reheated to 1250°C and hot rolled, after five passes reduction, each of which was 27.5%, to 5 mm (0.2 inch), with the finishing temperature of 920°C. After finishing rolling, the steels were surface ground to 3mm (0.12 inch). The strips were coiled at 650°C or 500°C afterward, followed

by cooling to room temperature. After hot rolling, the hot rolled coils were cold rolled to the thickness of 1.25 mm (0.05 inch) with 58% cold reduction or to the thickness of 0.85 mm (0.03 inch) with 72% cold reduction.

In order to define optimum annealing temperature, four cold rolled steels 5M (CT=500°C, CR=58%), 6M (CT=650°C, CR=58%), 5N (CT=500°C, CR=72%) and 6N (CT=650°C, CR=58%) were reheated to four annealing temperatures (790°C, 770°C, 750°C and 730°C) at 5°C/s. And after soaking for 60s, they were water quenched to room temperature. The volume fraction of martensite were measured (given in Table 4.2) and plotted in Figure 4.1. The dual-phase steels containing 50% - 60% volume fraction of martensite had a combination of high tensile strength and good ductility, and after full annealing process, 10% - 15% martensite would be lost. Therefore, 60% - 80% volume fraction of austenite was desirable during intercritical annealing and after full annealing process some austenite would transform into non-martensitic structures and 50%-60% of martensite would be formed. From the pre-annealing treatment results, V_m of dual-phase steels annealed at 770°C and 750°C ranged from 60% to 80%, so 770°C and 750°C were chosen as annealing temperatures.

Table 4.2 Defining optimum annealing temperature

Designation	CT (°C)	CR (%)	IAT (°C)	V _m (%)
5M	500	58	790	77.81
6M	650	58	790	72.03
5N	500	72	790	88.51
6N	650	72	790	84.49
5M	500	58	770	69.82
6M	650	58	770	67.26
5N	500	72	770	77.81
6N	650	72	770	74.00
5M	500	58	750	59.57
6M	650	58	750	52.12
5N	500	72	750	57.42
6N	650	72	750	59.44
5M	500	58	730	-
6M	650	58	730	41.83
5N	500	72	730	-
6N	650	72	730	45.92

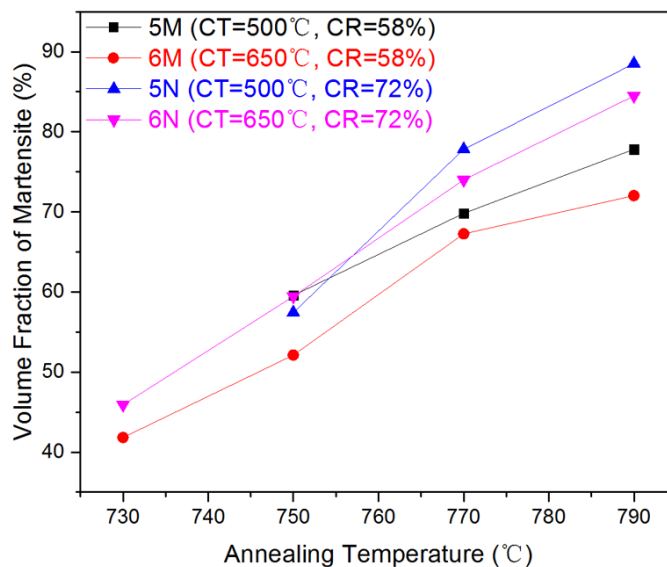


Figure 4.1 Volume fractions of martensite at different annealing temperatures

After cold rolling, these steels were machined and prepared for the simulation of annealing process, using a 3800 Gleeble. There were two annealing process in this study; one was standard galvanizing (F1) and the other one was supercool processing (G1), shown in the Figure 4.2. In each of two annealing paths, the samples were reheated to 770°C or 750°C at a heating rate of 5°C/s and soaked for 60s, followed by cooling down to different temperatures at a cooling rate of 15°C/s. In standard galvanizing, the steels were cooled to zinc pot temperature (460°C), followed by holding for 15s, and cooled to room temperature at a cooling rate of 10°C/s afterward. In supercool processing, the samples were cooled to 200°C, and after being held for 20s, they were up quenched to 460°C and held for 15s. After soaking, the steels were cooled to room temperature at 10°C/s. In terms of standard galvanizing, there was a three-stage cooling from intercritical annealing temperature (IAT) to room temperature, shown in Figure 4.2. The purpose of stage one (fast cooling from IAT to Zinc pot temperature) was to avoid the formation of new ferrite; stage two (a short holding time at zinc pot temperature) was designed to avoid the

formation of new bainite; stage three (fast cooling from zinc pot temperature to room temperature) aimed to form more martensite. For supercool processing, there was a five-stage treatment from IAT to room temperature. Stage one (fast cooling from IAT to supercool temperature) was designed to avoid the formation of new ferrite; the purpose of stage two (20 seconds holding at supercool temperature) was to form more martensite; stage three (up quenching from supercool temperature to zinc pot temperature) aimed to form tempered martensite; the goal of stage four (a short holding time at zinc pot temperature) was to avoid the formation of new ferrite and bainite; stage five (fast cooling from zinc pot temperature to room temperature) was to obtain more fresh martensite.

In this study, five factors should be taken into consideration based on both chemical compositions and thermomechanical process.

- 1) Compositions (0.15 w.t% carbon, high chromium, high molybdenum and addition of vanadium)
- 2) Coiling temperature (650°C and 500°C)
- 3) Cold reduction (58% and 72%)
- 4) Annealing temperature (770°C and 750°C)
- 5) Annealing path (standard galvanizing and supercool processing)

In terms of intercritical annealing, critical temperatures were predicted by JMatPro. There were two CCT curves of new austenite shown in Figure 4.3. The left one was the CCT curve of intercritical austenite with annealing temperature of 750°C; the right one was the CCT curve of intercritical austenite annealed at 770°C. Taking the annealing temperature of 770°C as an example, the equilibrium at A_{C3} ($A_{C3}=770^{\circ}\text{C}$) was assumed. The red line represented the behavior of intercritical austenite during cooling. From 770°C to zinc pot temperature, the

cooling rate was $15^{\circ}\text{C}/\text{s}$ and this fast cooling rate avoided the formation of new ferrite; at zinc pot temperature, there was a short time holding, which avoided the formation of new bainite; from zinc pot temperature to room temperature, the fast cooling with cooling rate of $10^{\circ}\text{C}/\text{s}$ ensured the formation of more martensite. In addition, the B_s , M_s , M_{50} and M_f temperatures were obtained from Figure 4.3 and given in Table 4.3

The tested samples were designated and given in Table 4.4, based on different coiling temperatures (CT), cold reduction (CR), intercritical annealing temperatures (IAT) and annealing paths.

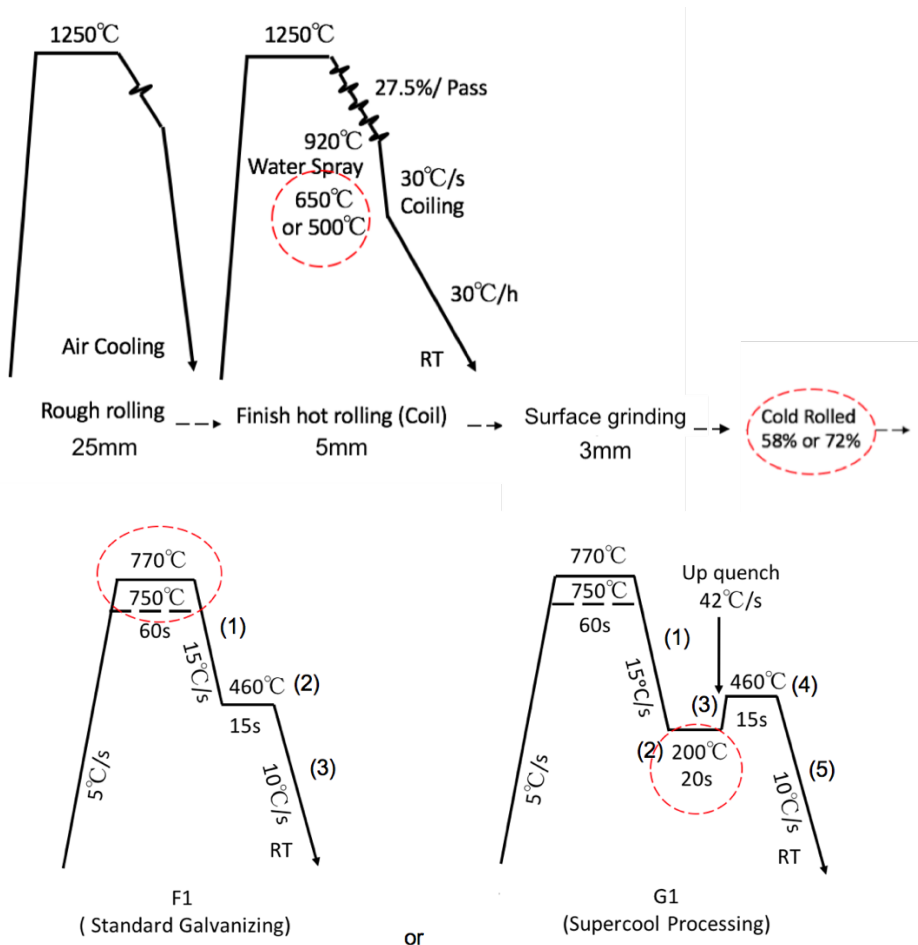


Figure 4.2. Schematic of thermomechanical process

Table 4.3 Critical temperatures of annealed dual phase steels, as the intercritical temperatures chosen 770°C and 750°C, estimated by JmatPro

IAT	B _s	M _s	M ₅₀	M ₉₀
770	491	319	284	202
750	459	281	244	159

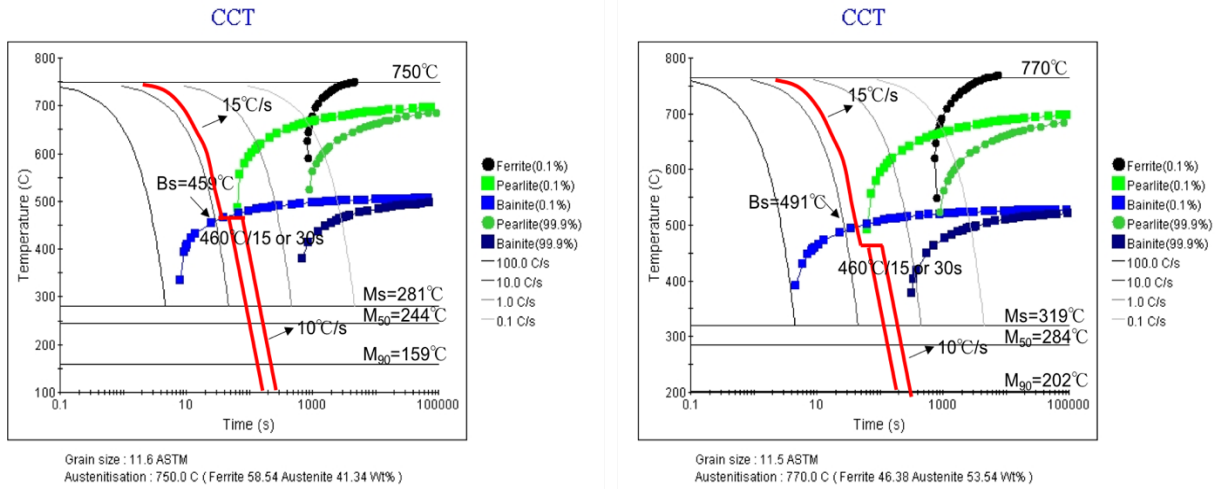


Figure 4.3 CCT of intercritical austenite during cooling, assuming the equilibrium at A_{C3} (770°C or 750°C)

Table 4.4 Designation of tested samples based on different coiling temperatures (CT), cold reduction (CT), and intercritical annealing temperatures (IAT)

Designation	CT(°C)	CR(%)	IAT(°C)	IHT(s)
5M7J	500	58	750	15
5M8J	500	58	770	15
6M7J	650	58	750	15
6M8J	650	58	770	15
5N7J	500	72	750	15
5N8J	500	72	770	15
6N7J	650	72	750	15
6N8J	650	72	770	15

4.3 EQUIPMENT AND FACILITIES

4.3.1 Optical microscopy

Optical microscopy, consisting of a system of lens, was applied to magnify and observe the microstructures of tested samples.

Samples were cut into tiny pieces by using a Buehler Isomet 1000 diamond cutting saw and mounted with Bakelite and copper powder. The mount was ground on silicon carbide abrasive paper, ranging from 600-1200 grit, followed by polishing with 0.05 μm alumina on polishing cloths in a vibrating polisher machine. After polishing, the surfaces of tested samples were etched by different etchants to reveal distinct microstructures. 2% Nital (98 ml pure ethanol mixed with 2 ml nitric acid) was applied to distinguish the ferrite and martensite, since it could help to reveal the ferrite grain boundary in low carbon steels. Lepera, a mixed solution of 50 ml of 1% $\text{Na}_2\text{S}_2\text{O}_5$ in distilled water and 50 ml of 4% picric acid in ethanol, was also utilized to reveal ferrite - martensite microstructures.

After sample preparation, a Sony digital camera attached to a Nikon Microscope, shown in Figure 4.4, was used to observe and capture the images of the microconstituent. ImageJ, an image analysis software, was applied to measure, calculate and analyze the average ferrite grain size and volume fraction of martensite, tempered martensite and bainite dependent on the OM images.

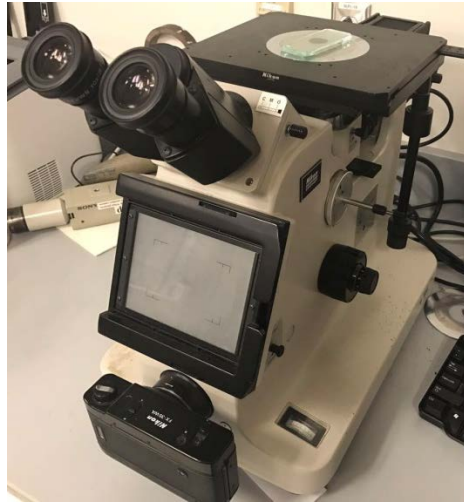


Figure 4.4 Sony digital camera attached to a Nikon Microscope

4.3.2 Scanning electron microscopy and electron backscatter diffraction

Although OM is widely regarded as an effective tool for metallurgical analysis, there are some special conditions where the images captured by OM are less useful. Because average ferrite grain sizes of tested samples were very small, the grain sizes could not be measured and calculated more precisely through the images captured by OM, even though the magnification of those images was 2000X. Besides ferrite and martensite, there were some other structures, such as bainite, retained austenite and tempered martensite, obtained in the final microstructures of tested samples. These microstructures would not be distinguished by OM, so morphology analysis needed to be used to reveal them.

ZEISS Sigma 500 VP SEM with Oxford Aztec X-EDS and FEI Apreo SEM, shown in Figure 4.5, were used in this research. The samples used in the SEM were ground, polished and etched by 2% Nital.



Figure 4.5 FEI Apreo SEM

Electron backscatter diffraction was also used in this study to obtain essential information, such as structure, crystalline orientation, stored energy, grain morphology, and dislocation density of tested samples. The scanned samples, after being ground and polished manually, were polished by vibrating polisher machine for more than four hours, in order that any scratches on the surface of the samples would be eliminated. The prepared samples were placed into the SEM chamber and tilted about 70° from the electron beam. The EBSD detector was inserted afterward, and in terms of EBSD scanning, 20kV voltage, 15 beam spot size and $0.1 \mu\text{m}$ step size were applied. After scanning, the EBSD data were analyzed by TSL OIM analysis software.

4.3.3 Tensile test

The tensile test provides significant mechanical properties, yield strength (YS), ultimate tensile strength (UTS), uniform elongation (UE), total elongation (TE) and n value (n) of the tested materials [67]. In this research, UTS and TE are two critical factors that are frequently used to

compare and select materials. The tested steels were cut and machined to subsize specimens based on ASTM E8 standard. Figure 4.6 shows the schematic of sheet tensile test samples.

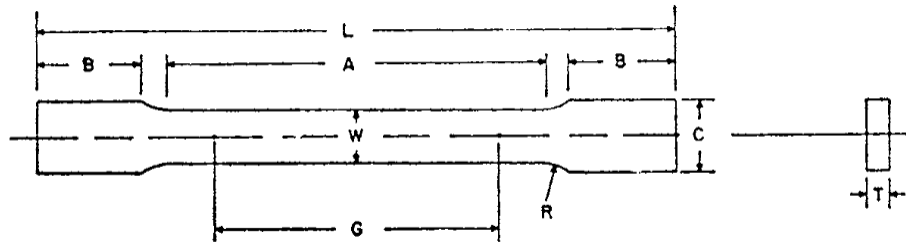


Figure 4.6 Schematic of sheet tensile test samples [68]

In Figure 4.6, G is gage length, W is the width of cross section, T is the thickness, R is radius of fillet, L is the total length of the sample, A is the length of reduced section, B is the length of grip section and C is the width of grip section [68]. In this study, original gage length was machined to 10 mm (0.4 in) and width of cross section was 6mm (0.24 in). The thickness varied with the cold reduction; the thickness was 1.25mm (0.05 in) with cold reduction of 58%, while the thickness was 0.85 (0.03 in) when cold reduction was 72%.

4.3.4 Vickers hardness test and nano hardness test

The Vickers hardness test provides the microhardness of tested materials, which has a roughly linear relationship with tensile strength. A Leco M-400 G microhardness tester was applied with a load of 300g. Five indents were performed on the quarter position of the surface of each tested specimen. The hardness data were collected by tester itself and the average and standard deviation of microhardness of each sample were calculated and analyzed by Excel math functions.

Nano hardness test was used to determine the hardness of both ferrite and martensite of steels in different pre-annealing conditions and annealing procedures and to find out the relationship between volume fraction of martensite and hardness of martensite. Compared with conventional Vickers hardness test, the load and the size of the nanoindenter are considerably smaller. Therefore, the nanoindentations can be placed in the center of both ferrite grains and martensite islands to ensure the accuracy of the data. Before testing, the polished samples were slightly etched by 2% Nital and observed by OM to find out the appropriate tested area, which was surrounded by several markers afterward, utilizing Vickers hardness tester. The samples were polished in vibrating polisher machine for several minutes to eliminate the etched surface, while the markers were remained. After sample preparation, specimens were tested by Hysitron TriboIndenter, shown in Figure 4.7. In each of tested steels, twenty-five nanoindenters were performed with a pattern of 5 rows \times 5 columns, and the spacing of each indenter is 4 μm with a load of 2000 μN . Furthermore, after testing, each sample was slightly etched again, and observed by SEM to examine the twenty-five nanoindentations.



Figure 4.7 Hysitron TriboIndenter

4.3.5 Hole expansion ratio test

Hole expansion ratio (HER) test is commonly used to evaluate the edge cracking resistance of advanced high strength steels (AHSS). It is a significant indicator for the shear edged ductility of dual phase steels.

In this study, the HER blanks were heat treated by Gleeble, followed by punching a hole of 10mm diameter in the center. Before testing, the initial diameters of punched holes were measured five times. Subsequently, HER blanks were placed on the testing apparatus [69] and deformed by a conical punch with a speed of 0.3mm/s. When a crack propagated the whole thickness of the HER blanks, the test was stopped. After test, the final diameters of holes were also measured five times. Thus, the hole expansion ratio can be expressed by Equation (4-1).

$$\lambda = \frac{D_f - D_o}{D_o} \times 100\% \quad (4-1)$$

where, λ is the hole expansion ratio, D_f is the hole diameter after test and D_o is the original hole diameter. The process of hole expansion test is shown in Figure 4.8.

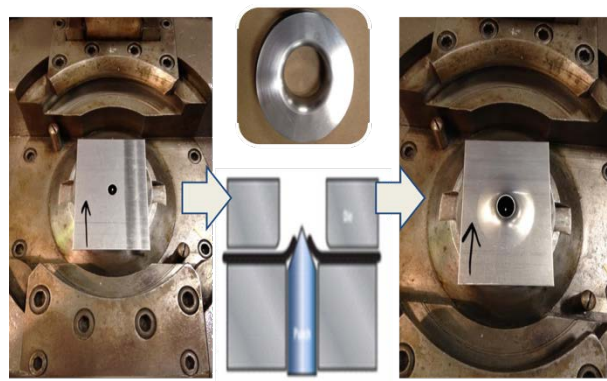


Figure 4.8 The schematic of hole expansion test procedure [69]

4.3.6 Vibrating sample magnetometer

To have accurate determination of volume fraction of retained austenite, a LakeShore vibrating sample magnetometer (VSM) was used in this study, shown in Figure 4.9. The saturation magnetization can be obtained in the magnetic curve and the volume fraction of retained austenite can be calculated by the difference of samples with and without retained austenite [70], since martensite, ferrite as well as cementite are ferromagnetic, while austenite is paramagnetic [71]. The volume fraction of retained austenite can be expressed by Equation (4-2).

$$f_{\gamma} = 1 - \beta \frac{M_s(c)}{M_s(f)} \quad (4-2)$$

where, f_{γ} is the volume fraction of retained austenite, $M_s(c)$ is the saturation magnetization of samples containing austenite, $M_s(f)$ is the saturation magnetization of samples without austenite and β is related to saturation magnetization of martensite, ferrite and cementite and the volume fraction of cementite [1]. When the volume fraction of cementite precipitates is negligible, the β can be regards as one.

The samples were machined into cubes with dimension of 1mm × 3mm × 5mm (thickness, width and length). In the VSM, samples were magnetized by a uniform field created between the electromagnetic poles, which caused samples to generate their own magnetic fields. When samples underwent sinusoidal motion, like mechanical vibration, the sensing of detection coils induced electric current in these coils. The sample's magnetic moment was measured by measuring electric current induced by detection coils. The volume fraction of retained austenite was calculated by the changes between the maximum magnetic moment of the sample containing austenite and that of sample without austenite.



Figure 4.9 LakeShore vibrating sample magnetometer

5.0 RESULTS

5.1 RESULTS OF COLD ROLLED STEELS

In the pre-annealing condition, the steels were designated dependent on the different coiling temperatures and cold reductions, as given in Table 5.1.

Table 5.1 Designation of cold rolled steels based on different coiling temperatures (CT) and cold reductions (CR)

ID	CT(°C)	CR(%)	ID	CT(°C)	CR(%)
5M	500	58	5N	500	72
6M	650	58	6N	650	72

The microstructures of received cold rolled DP steels are shown in Figure 5.1. Figure 5.1 a) and b) represent the cold rolled steels with the same low cold reduction (58%) but with different coiling temperatures. In the higher coiling temperature (650°C), the microstructures consist of polygonal ferrite, pearlite and bainite. The ferrite grains are coarser and the amount of pearlite is larger than the cold rolled steels with lower coiling temperature (500°C). In terms of lower coiling temperature, acicular ferrite, pearlite, and bainite can be observed in the final microstructures. It is obvious that, after 58% cold reduction, ferrite and pearlite are elongated along the rolling direction in the microstructures of cold rolled steels with different coiling temperatures.

Furthermore, Figure 5.1 c) and d) show the cold rolled steels with the same higher cold reduction (72%) but with different coiling temperatures. Compared with lower cold reduction, the ferrite grains and pearlite are deformed and elongated remarkably, the ferrite grains are compressed so tightly that ferrite grain boundaries are not easily observed.

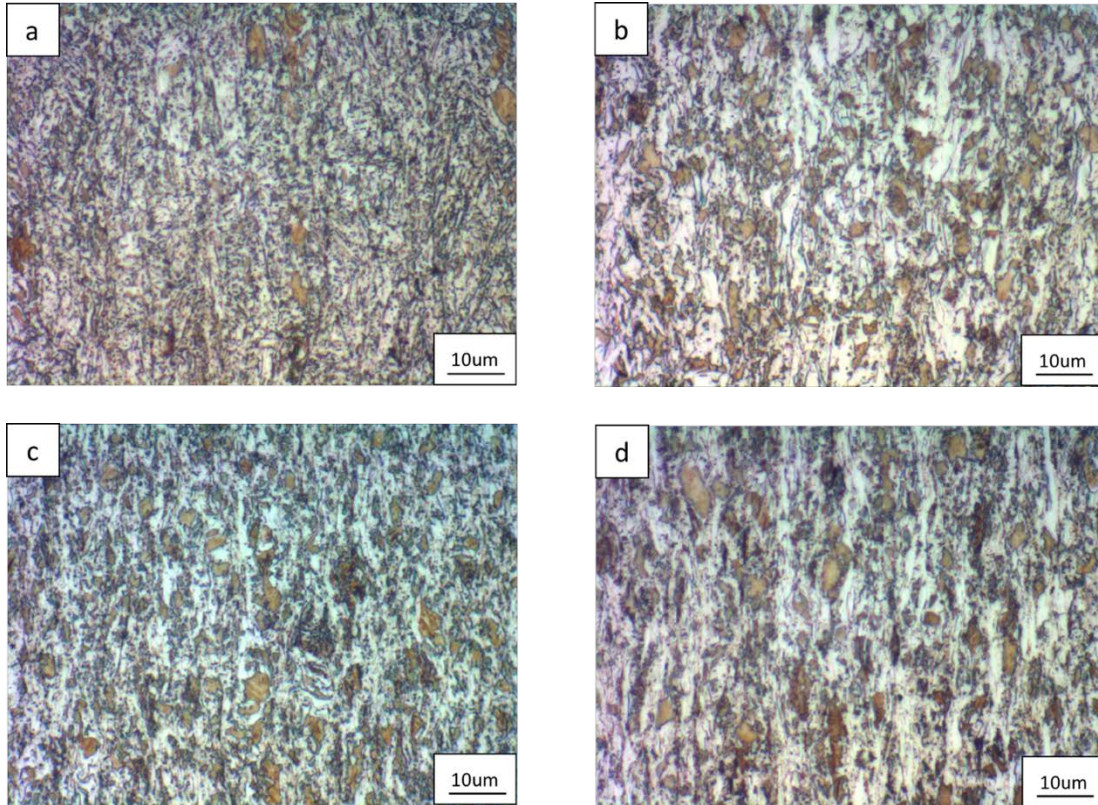


Figure 5.1 OM images of microstructures of cold rolled steels, etched by 2% Nital, a) 5M (CT=500°C, CR=58%), b) 6M (CT=650°C, CR=58%), c) 5N (CT=500°C, CR=72%), d) 6N (CT=650°C, CR=72%)

Table 5.2 Vickers hardness (300gf) of cold rolled steels with different coiling temperatures (CT) and cold reductions (CR)

ID	CT(°C)	CR(%)	VHN(HV)	ID	CT(°C)	CR(%)	VHN(HV)
5M	500	58	369±6	5N	500	72	406±5
6M	650	58	360±6	6N	650	72	395±7

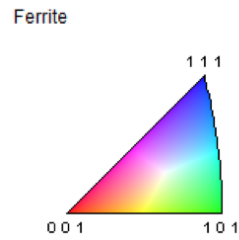
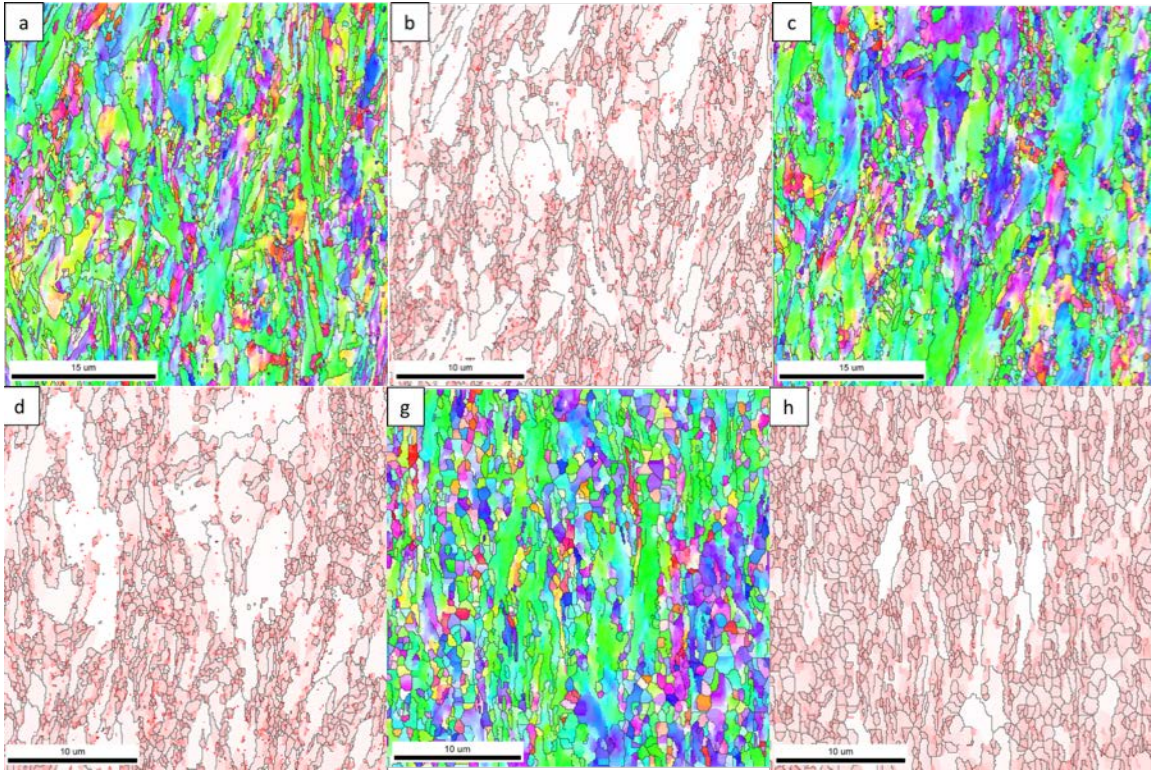


Figure 5.2 Stored energy of cold rolled steels, a) 5M (CT=500°C, CR=58%) IPF (with HAGB), b) 5M SE=5.01J/cm³, c) 6M (CT=650°C, CR=58) IPF (with HAGB), d) 5M SE=5.13J/cm³, e) 5N (CT=500°C, CR=58%) IPF (with HAGB), f) 5N SE=5.72J/cm³, g) 6N (CT=650°C, CR=72%) IPF (with HAGB), h) 6N SE=5.60J/cm³

Table 5.3 Stored Energy (J/cm³) in Cold Rolled Steels Before Annealing

ID	CT(°C)	CR(%)	GB	Matrix	Total
5M	500	58	0.56	5.01	5.57
6M	650	58	0.52	5.13	5.65
5N	500	72	0.75	5.72	6.47
6N	650	72	0.72	5.60	6.32

The inverse pole figures of cold rolled steels are given in Figure 5.2 a), c), e) and g), and the meaning of different colors are represented by the color triangle at the end of the Figure 5.2. When the cold reduction is 58%, the ferrite grains are deformed along the rolling direction. Figure 5.2 a) and b) compare the ferrite grain sizes at different coiling temperatures, illustrating that the higher coiling temperature results in ferrite grain coarsening. It is obvious that ferrite grains are deformed and elongated more along the rolling direction with the increasing of the cold reduction from Figure 5.2 a) and c). The ferrite grains are highly compressed when the hot rolled coils are 72% cold rolled. The stored energy, the combination of sub-grain method and EBSD data of cold rolled steels are shown in Figure 5.1.2 b), d), f) and h), and it is obvious that the combination of low coiling temperature and high cold reduction can have the highest stored energy, which could provide more driving force for the formation of austenite [1] and ferrite recrystallization at a short time during intercritical annealing. The stored energies of grain boundary and matrix are given in Table 5.3. Because stored energy is the sum of the energy stored in the grain boundaries and sub-grain boundaries in the ferrite matrix. From Table 5.3, the combination of low coiling temperature and high cold reduction had the highest stored energy both in grain boundaries and sub-grain boundaries in ferrite center.

5.2 RESULTS OF ANNEALED STEELS

5.2.1 Mechanical Properties

All the engineering stress-strain curves of annealed steels with different coiling temperatures, cold reductions, intercritical annealing temperatures and annealing paths are represented in Figure 5.3 and Figure 5.4.

Figure 5.3 left and Figure 5.4 left show the engineering stress and strain curves with low cold reduction (58%) and Figure 5.3 right and Figure 5.4 right represent the engineering stress and strain curves with high cold reduction (72%). And from these four figures, the tensile strengths of specimens with 72% cold reduction are higher than those of steels with 58% cold reduction, while the total elongations with different cold reductions are similar.

According to these four figures, the red flow curves and blue flow curves stand for the steels annealed at high intercritical annealing temperature (770°C); while green and black curves represent the specimens annealed at low intercritical annealing temperature (750°C). It is obvious that the tensile strengths of steels annealed at high annealing temperature (770°C) are higher than the those of steels annealed at low annealing temperature (750°C).

When compared with the flow curves of samples with supercool processing (G1), those of steels annealed by standard galvanizing (F1) have higher tensile strength and lower total elongation. All these differences are due to different final microstructures, volume fraction of different phases and grain sizes, which will be discussed below.

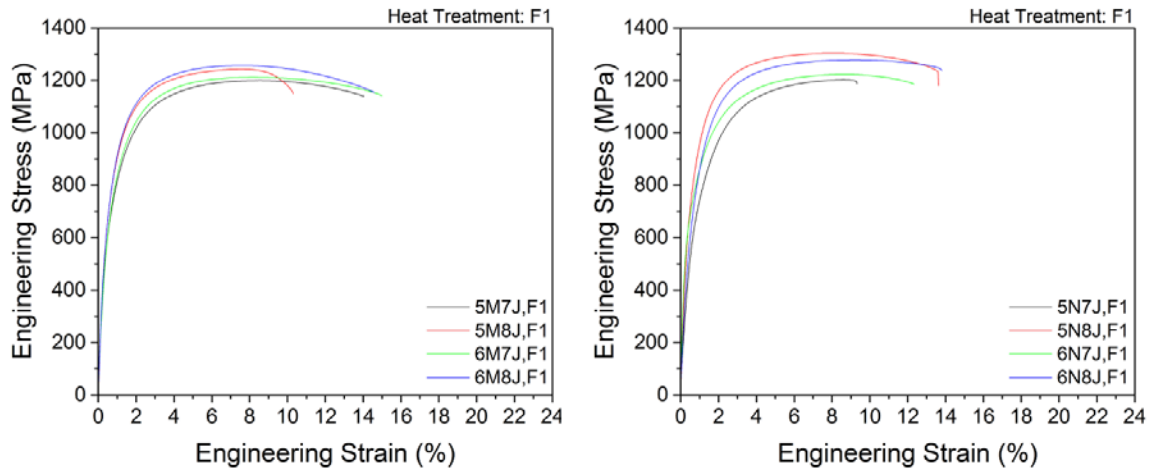


Figure 5.3 Engineering stress-strain curve of annealed steels with cold reduction of 58% (left) and cold reduction of 72% (right) annealed by standard galvanizing (F1)

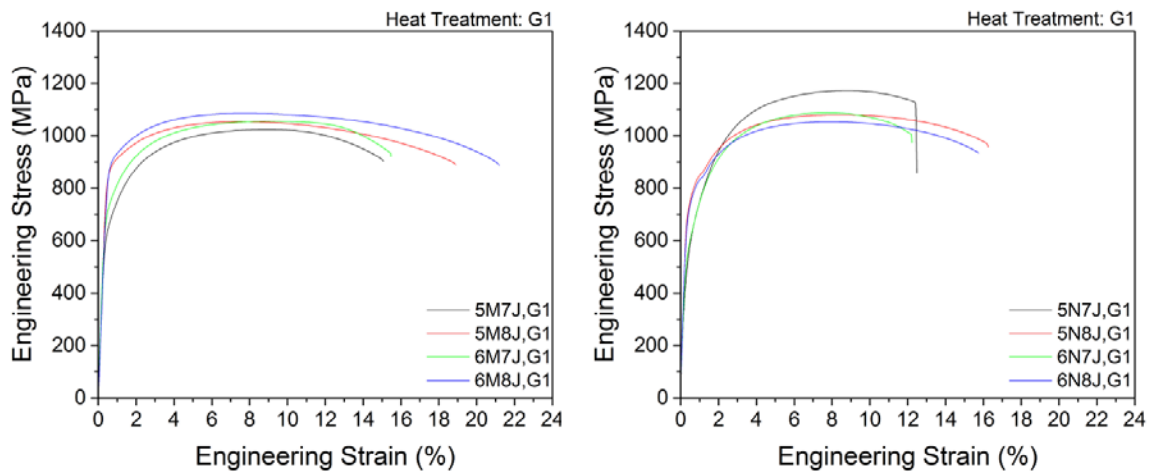


Figure 5.4 Engineering stress-strain curve of annealed steels with cold reduction of 58% (left) and cold reduction of 72% (right) annealed by supercool processing (G1)

Tensile strength (UTS)

All the tensile strengths of different coiling temperatures, cold reductions, intercritical annealing temperatures, and annealing paths are plotted in Figure 5.5. It is obvious that all the tensile

strengths are above 1000MPa and all the dual-phase steels reach the minimum level of DP980. The whole tensile strengths of dual-phase steels annealed by standard galvanizing are above 1150 MPa, and 5N8J (CT=500°C, CR=72%, IAT=770°C, IHT=15s) even reaches 1303MPa.

In Figure 5.5, red bars show the tensile strengths of steels annealed at low annealing temperature (750°C) and blue bars represent the tensile strengths of steels annealed at high annealing temperature (770°C). The blue bars are always higher than the red sparse bars, except for 5N7J, G1 and 5N8J, G1. Thus, the high annealing temperature (770 °C) can lead to higher strength than the low annealing temperature (750°C), because, according to the level rule, when intercritically annealed at 770 °C, more austenite is formed and after cooling and more martensite is found in the final microstructure.

In Figure 5.5, the designations of cold reductions are different; M stands for 58% cold reduction and N shows 72% cold reduction. UTS of 5M8J, F1 is 1242 MPa and UTS of 5N8J, F1 is 1303MPa, so UTS of 5M8J, F1 is less than 5N8J, F1. In terms of supercool processing, UTS of 5M7J, G1 is 1024MPa and UTS of 5N7J, G1 is 1173 MPa, so UTS of 5M7J, G1 is less than 5N7J, F1. Therefore, high cold reduction (72%) can give us more tensile strength than the low cold reduction (58%).

The effect of coiling temperature on the strength might be related to cold reduction. When the cold reduction is 58%, the tensile strengths of steels with coiling temperature of 650°C are higher than those of steels with coiling temperature of 500°C, even though the ferrite grains of 650°C are coarser than those of 500°C and the volume fraction of martensite of 650°C is less than that of 500°C. This may be attributed to the precipitates in ferrite matrix. When the cold

reduction is 72%, however, the tensile strengths of steels with coiling temperature of 500°C are higher than those of steels with coiling temperature of 650°C.

The effect of annealing paths on tensile strength can be obtained in Figure 5.5. It is obvious that for same designation, the tensile strength of the steel annealed by standard galvanizing is higher than that of the steel annealed by supercool processing. For example, UTS of 5M7J, F1 is 1200MPa, and UTS of 5M7J, G1 is 1024MPa, so UTS of 5M7J, F1 is more than UTS of 5M7J, G1. It is attributed to different final microstructures. In the GI process, the final microstructure consists of ferrite, martensite and retained austenite and the volume fraction of martensite ranges from 45% to 55%. While in terms of supercool processing, the final microstructure comprises ferrite, martensite, tempered martensite and retained austenite. The volume fraction of fresh martensite ranges from 5% to 15% and a large amount of the structure is tempered martensite. From Davies' theory, the tensile strength is dependent on the volume fraction of fresh martensite. Therefore, the steels annealed by GI are stronger than those annealed by supercool processing.

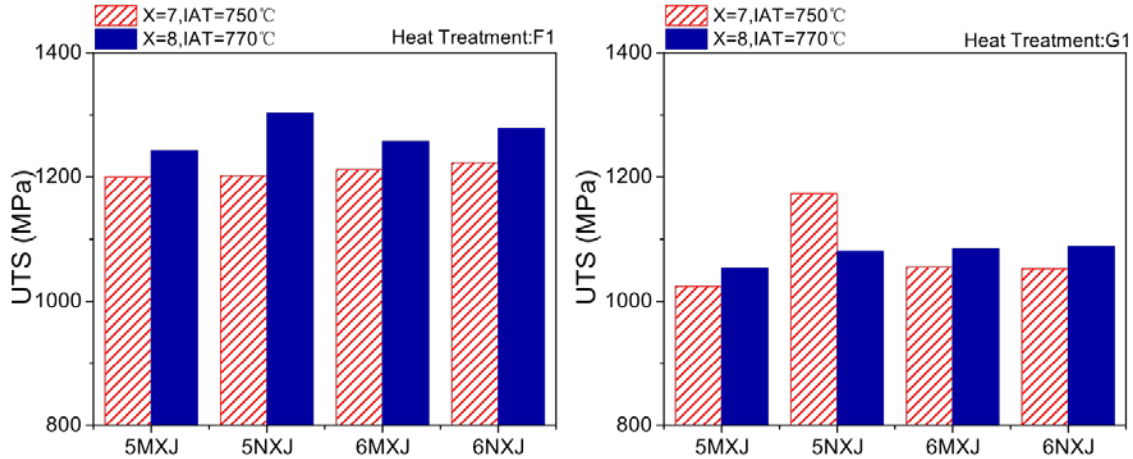


Figure 5.5 Ultimate tensile strength (UTS) of dual phase steels annealed by standard galvanizing (F1) and supercool processing (G1), in terms of each of annealing process, 5 represents CT=500°C, 6 means CT=650°C, M indicates CR=58%, N is CR=72%, X=7 IAT=750°C and X=8 IAT=770°C

Yield strength (YS)

Figure 5.6 shows the yield strengths of dual-phase steels; the left figure stands for the steels annealed by standard galvanizing and the right one represents the steels annealed by supercool processing. The tensile strengths are also controlled by several factors.

The yield strengths of steels annealed at 770°C are higher than those of steels with annealing temperature of 750°C. Because, from the level rule, higher annealing temperatures lead to a greater volume fraction of austenite, and, after cooling, more martensite would be formed, compared with lower annealing temperature. From Davies' theory, the yield strength is also dependent on volume fraction of martensite. Thus, the yield strength improves as the annealing temperature increases.

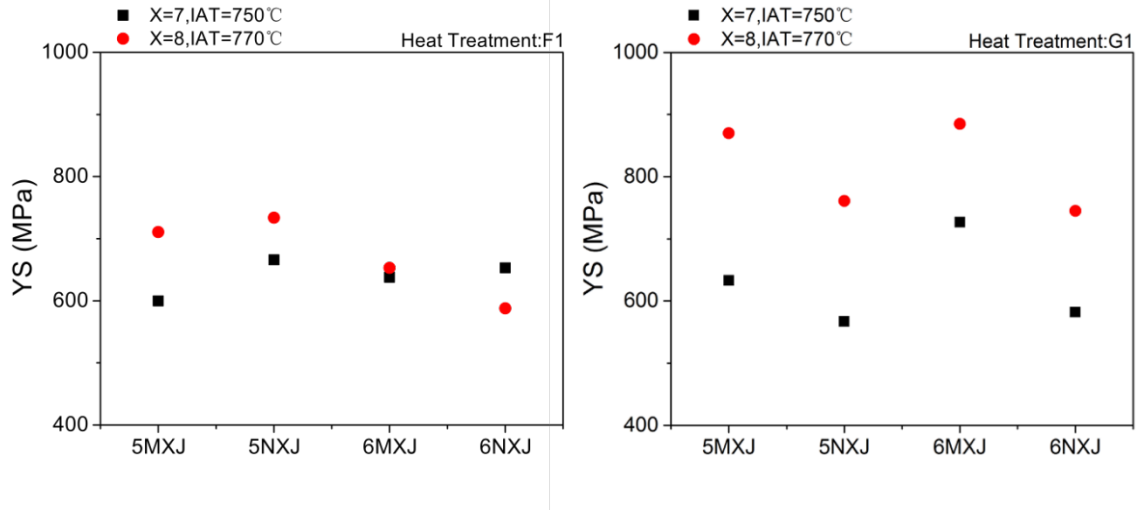


Figure 5.6 Yield strength (YS) of dual phase steels annealed by standard galvanizing (F1) and supercool processing (G1), in terms of each of annealing process, 5 represents CT=500°C, 6 means CT=650°C, M indicates CR=58%, N is CR=72%, X=7 IAT=750°C and X=8 IAT=770°C

Yield strength to tensile strength ratio (YS/UTS)

Figure 5.7 shows the yield strength to tensile strength ratios (YS/UTS) of dual-phase steels annealed by standard galvanizing and supercool processing. In standard galvanizing procedure, the YS/UTS ratios of samples remain the similar. While, in terms of supercool processing, the YS/UTS ratios of annealed steels range from 0.5 to 0.9.

From Figure 5.7, it is obvious that the YS/UTS ratios of steels with low cold reduction (58%) are higher than those of steels with high cold reduction (72%), since the tensile strengths of dual-phase steels with low cold reduction (58%) are lower, compared with the those of dual-phase steels with high cold reduction (72%). In addition, the YS/UTS ratio is also controlled by annealing temperature. In terms of supercool processing, the YS/UTS ratios of steels annealed at 770°C are higher than those of steels annealed at 750°C, and the high coiling

temperature results in larger amount of martensite, which indicates that YS/UTS ratio is also dependent on the volume fraction of martensite.

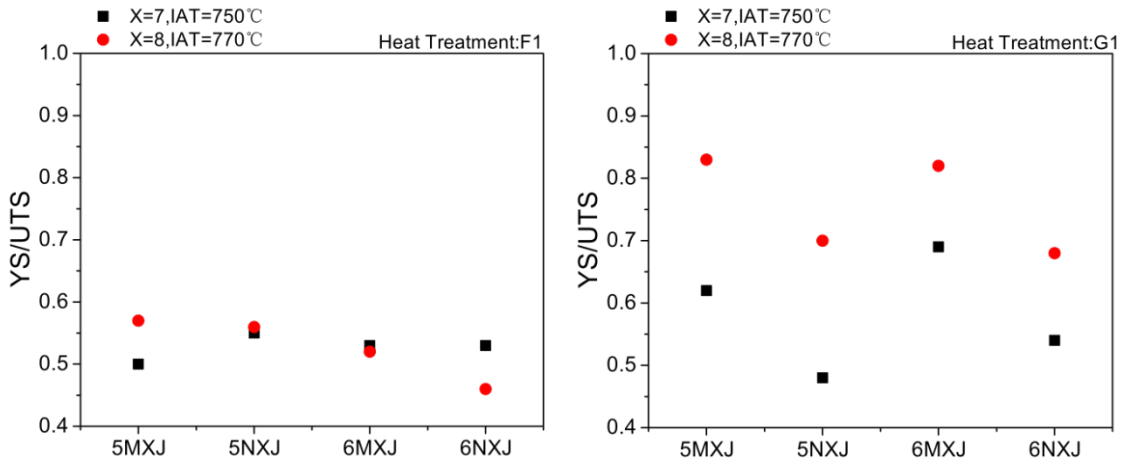


Figure 5.7 YS/UTS of dual phase steels annealed by standard galvanizing (F1) and supercool processing (G1), in terms of each of annealing process, 5 represents CT=500°C, 6 means CT=650°C, M indicates CR=58%, N is CR=72%, X=7 IAT=750°C and X=8 IAT=770°C

Total Elongation (TE)

The total elongations (10 mm gage length) of all steels are shown in Figure 5.8. Compared with the total elongation with high cold reduction (72%), TE with low cold reduction (58%) is higher. In supercool processing, TE of high annealing temperature (770°C) is larger than that of low annealing temperature (750°C), indicating in terms of supercool processing, the high annealing temperature (770°C) not only improves the tensile strength, but it can also increase the total elongation. For annealing paths, compared with TE of steels annealed by standard galvanizing, the total elongation of steels annealed by supercool processing is higher, since the volume fraction of martensite of samples with GI is larger than that of steels with supercool processing.

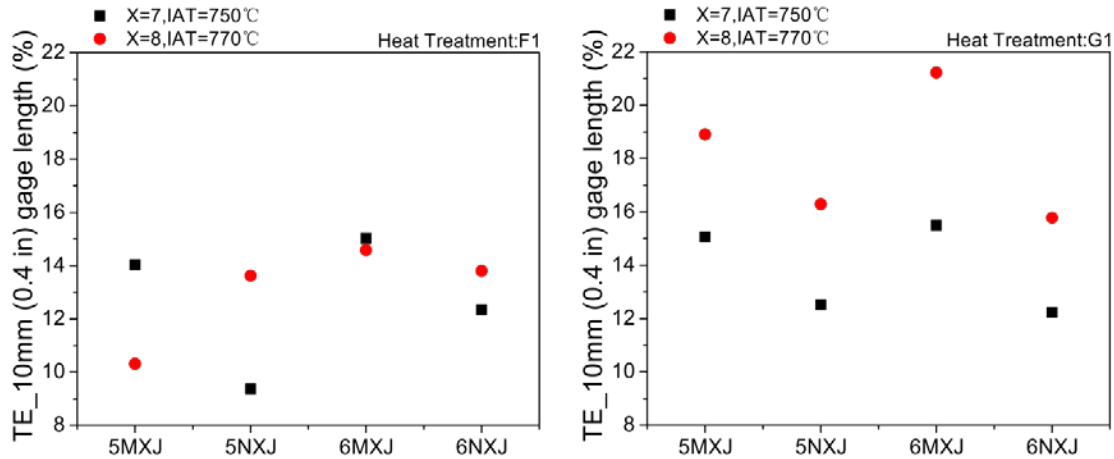


Figure 5.8 Total elongation (TE) of dual phase steels annealed by standard galvanizing (F1) and supercool processing (G1), in terms of each of annealing process, 5 represents CT=500°C, 6 means CT=650°C, M indicates CR=58%, N is CR=72%, X=7 IAT=750°C and X=8 IAT=770°C

Figure 5.9 has important implication for developing the relationship between total elongation (10mm gage length) and tensile strength of dual-phase steels annealed by standard galvanizing and supercool processing. And the data in Figure 5.9 are all from Table 5.4 and Table 5.5. The blue solid line shows that the product of TE×UTS is 10K MPa × %. The red dashed line represents the product of TE×UTS is 18K MPa × %. The green dotted line illustrates the product of TE×UTS is 22K MPa × %. The region between 10K and 18K MPa × % is DP steel; TRIP steel lies between 18K and 22K MPa × % lines; the area above 22K MPa × % line is the AHSS Generation III steel zone. From the Figure 5.9, in GI process, the majority of the steels lie in the DP area, while four steels, 5M8K (CT=500°C, CR=58%, IAT=770°C and IHT=30s), 6M7J (CT=650°C, CR=58%, IAT=750°C and IHT=15s), 6M8J (CT=650°C, CR=58%, IAT=770°C and IHT=15s), 6N7K (CT=650°C, CR=72%, IAT=750°C and IHT=30s) are in the TRIP region. In terms of supercool processing, although the most part of annealed steels are in the DP area, 5M8J

(CT=500°C, CR=58%, IAT=770°C and IHT=15s) lies in the TRIP area and 6M8J (CT=650°C, CR=58%, IAT=770°C and IHT=15s), illustrating that these two steels have both high tensile strength and fine ductility.

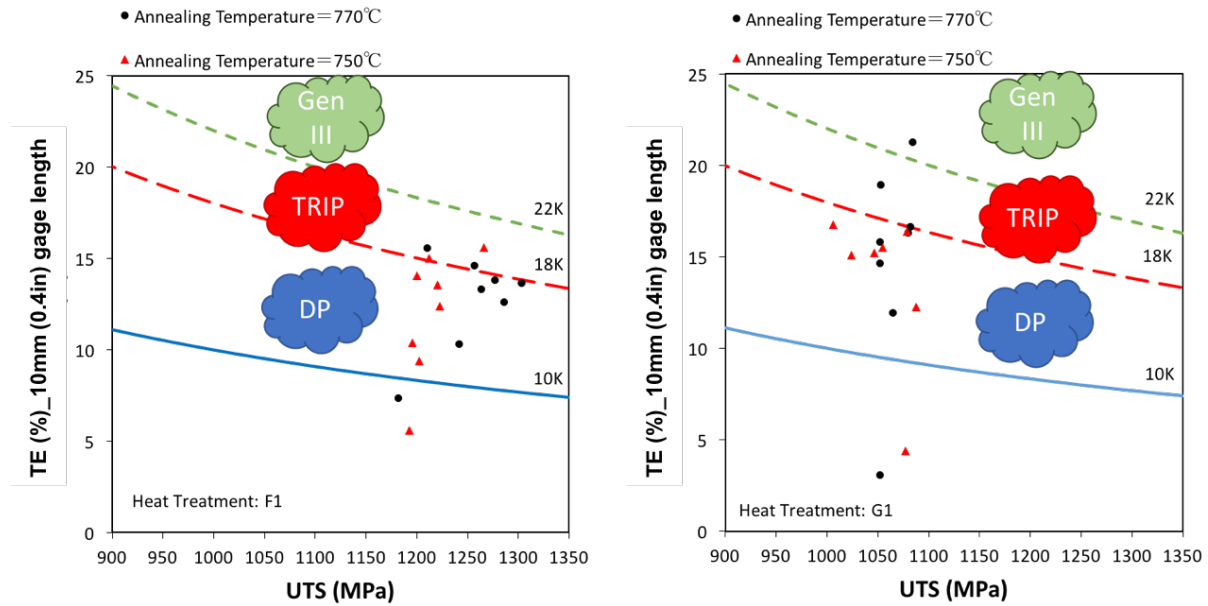


Figure 5.9 The relationship between total elongation and tensile strength of dual phase steels annealed by standard galvanizing (F1) and supercool processing (G1), blue solid line shows the minimum product of TE×UTS for DP steels (10K), red dashed line represents the minimum product of TE×UTS for TRIP steels (18K), and green dotted line indicates the minimum product of TE×UTS for Generation III steels (22K)

Table 5.4 Mechanical properties (UTS, YS, TE, YS/UTS, UTS×TE) of the annealed steels with standard galvanizing

(F1)

Designation	UTS (MPa)	YS (MPa)	TE (%)_10mm gage length	YS/UTS	UTS×TE (MPa×%)
5M7J, F1	1200	600	14.04	0.50	16847
5M8J, F1	1242	711	10.31	0.57	12805
5N7J, F1	1202	666	9.37	0.55	11270
5N8J, F1	1303	734	13.63	0.56	17765
6M7J, F1	1212	638	15.02	0.53	18197
6M8J, F1	1257	653	14.59	0.52	18343
6N7J, F1	1223	653	12.35	0.53	15105
6N8J, F1	1278	588	13.81	0.46	17647

Table 5.5 Mechanical properties (UTS, YS, TE, YS/UTS, UTS×TE) of the annealed steels with supercool processing

(G1)

Designation	UTS (MPa)	YS (MPa)	TE (%)_10 mm gage length	YS/UTS	UTS×TE (MPa×%)
5M7J, G1	1024	633	15.06	0.62	15421
5M8J, G1	1053	870	18.91	0.83	19906
5N7J, G1	1173	567	12.52	0.48	14677
5N8J, G1	1080	761	16.30	0.70	17608
6M7J, G1	1055	727	15.49	0.69	16336
6M8J, G1	1085	885	21.23	0.82	23031
6N7J, G1	1088	582	12.24	0.54	13316
6N8J, G1	1052	745	15.78	0.71	16607

Hole expansion ratio (HER)

Hole expansion ratio test is commonly used to evaluate the edge cracking resistance of advanced high strength steels (AHSS). It is a significant indicator for the shear edged ductility of dual phase steels.

From Table 5.4 and Table 5.5, 6 dual-phase steels have good products of $UTS \times TE$ (MPa \times %). These 6 steels were sectioned for hole expansion ratio (HER) test. Table 5.6 lists their RA, HER, UTS, TE and $UTS \times TE$ properties. The hole expansion ratios of dual phase steels annealed by supercool processing are higher than those of steels annealed by standard galvanizing, which might be attributed to the large amount of tempered martensite and retained austenite obtained in the final microstructures after supercool processing. Figure 5.10 (a) plots the RA and HER in Table 5.6, which indicates that the hole expansion ratio and the reduction in area has a linear relation, since HER represents the sheared edge ductility related to the post uniform elongation and reduction in area [1]. After using fitting curve function of ORIGIN 2016, the relationship between HER of steels annealed by standard galvanizing and RA can be expressed by Equation (5-1). The relationship between HER of steels annealed by supercool processing and RA can be expressed by Equation (5-2).

$$HER=16.17-0.21 \times RA \text{ (\%)} \quad (5-1)$$

$$HER=-17.99+1.56 \times RA \text{ (\%)} \quad (5-2)$$

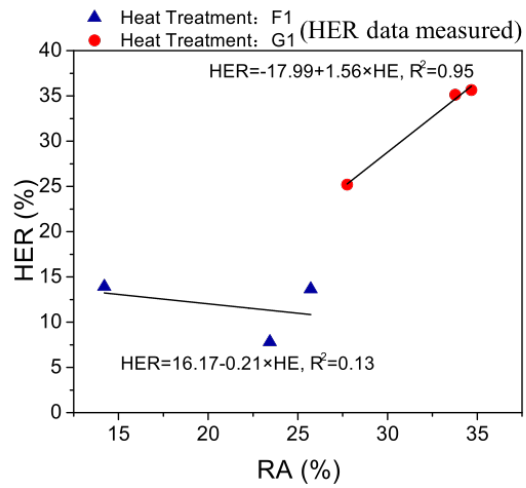
The hole expansion ratios of all the dual-phase steels can be estimated by this Equation (5-1) and Equation (5-2), and the results are given in Table 5.7. Figure 5.10 (b) represents the relationship between hole expansion ratios and tensile strengths of dual-phase steels annealed by supercool processing (G1). This figure indicates that increasing the tensile strength, the HER would be sacrificed.

Table 5.6 RA, HER, UTS, TE and UTS×TE of dual phase steels

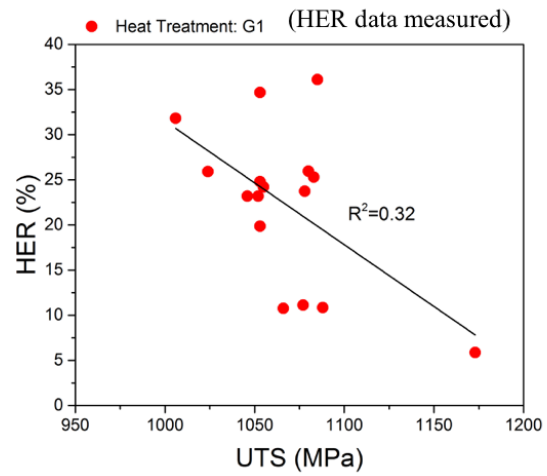
Designation	RA (%)	HER (%)	UTS (MPa)	TE (%)_10mm gage length	UTS×TE (MPa×%)
5M8K, F1	25.72	13.65	1211	15.54	18819
6M8J, F1	23.44	7.8	1257	14.59	18343
6N7K, F1	20.64	14.21	1266	15.60	19747
5M8J, G1	33.77	35.13	1054	18.91	19906
6M8J, G1	34.67	35.65	1085	21.23	23031
6M8K, G1	27.75	25.21	1083	16.62	17995

Table 5.7 RA, HER (predicted from RA data), UTS, of dual phase steels

Designation	RA (%)	HER (%)	UTS (MPa)	Designation	RA (%)	HER (%)	UTS (MPa)
5M7J, F1	20.48	11.87	1200	5M7J, G1	28.13	25.90	1024
5M7K, F1	16.48	12.71	1220	5M7K, G1	31.92	31.81	1006
5M8J, F1	20.00	11.97	1242	5M8J, G1	33.77	34.68	1053
5M8K, F1	25.72	10.77	1211	5M8K, G1	24.27	19.86	1053
5N7J, F1	11.82	13.69	1212	5N7J, G1	15.30	5.88	1173
5N7K, F1	12.48	13.55	1193	5N7K, G1	18.66	11.13	1077
5N8J, F1	16.43	12.72	1303	5N8J, G1	28.17	25.95	1085
5N8K, F1	15.34	12.95	1286	5N8K, G1	18.43	10.76	1080
6M7J, F1	22.01	11.55	1212	6M7J, G1	27.05	24.21	1055
6M7K, F1	19.34	12.11	1195	6M7K, G1	26.41	23.20	1046
6M8J, F1	23.44	11.25	1257	6M8J, G1	34.67	36.10	1085
6M8K, F1	22.00	11.55	1182	6M8K, G1	27.75	25.30	1083
6N7J, F1	18.80	12.22	1223	6N7J, G1	18.49	10.85	1088
6N7K, F1	13.92	13.25	1266	6N7K, G1	26.75	23.74	1078
6N8J, F1	19.79	12.01	1278	6N8J, G1	26.40	23.19	1052
6N8K, F1	20.61	11.84	1264	6N8K, G1	27.44	24.81	1053



(a)



(b)

Figure 5.10 The relationship among hole expansion ratios (HER), tensile strength (UTS) and reductions in area (RA). (a) HER (measured) vs RA; (b) HER (predicted from RA) vs UTS

Work hardening behavior

Work hardening exponent is one of the most useful engineering materials properties, describing the materials resistance to continuous deformation. It is not only a critical factor for evaluating cold forming performance of a metal sheet but a significant element for the selection of stamping parts.

Work hardening exponent can be described as the Hollomon Equation (5-3).

$$\sigma = K\varepsilon^n \quad (5-3)$$

where, σ is true stress, K is strength coefficient, ε is true strain and n is work hardening exponent. So, n value, the rate of strain hardening can be obtained from the slope of the flow curve, representing the working hardening behavior of dual-phase steels. It can be calculated by $n = \frac{d\ln(\sigma)}{d\ln(\varepsilon)}$. From n vs engineering curve, the n values keep constant at 4%-6% engineering strain, so after linearly fitting $\ln\sigma$ - $\ln\varepsilon$ curves, all the n values at 4%-6% engineering strain of dual phase steels annealed by standard galvanizing (F1) and supercool processing are given in Table 5.8 and the uniform elongations (10 mm gage length) of these steels are also included. From Figure 5.11 (a) and (b), increasing the annealing temperature develops the n value and the high cold reduction leads to high work hardening ratio. Furthermore, the relationship between uniform elongations and the n values of the whole annealed steels are illustrated in Figure 5.11 (c). It is obvious the uniform elongations and strain hardening ratios of DP steels have a linear relationship expressed by Equation (5-4) with $R^2=0.72$, indicating UE (10 mm gage length) and n value have a strong linear relation. Therefore, the higher the work hardening exponent is, the more material would be hardened and deformed before necking.

$$UE=4.52+31.26 \times n \quad (5-4)$$

The work hardening ratio of annealed steels at 0.2%-0.5% engineering strain are given in Table 5.8. The n_1 values are higher than n_2 , indicating that the dual-phase steels in this research obeyed the two-stage work hardening mechanism, and the work hardening ratio of the initial strain range is higher than that of the high strain range. The work hardening ratio of the first stage was attributed to the deformed ferrite. When ferrite grains with high dislocation density were deformed near the ferrite/martensite interface regions in the first stage, the vanadium carbide precipitates retarded the movement of dislocations, thereby increasing the strain hardening rate of the first stage. As a result, the n value of first stage is twice more than the work hardening rate of the second stage. In the second stage, the co-deformation of ferrite and martensite or tempered martensite contributed to the strain hardening.

Table 5.8 Work hardening behavior n_1 (0.2%-0.5% engineering strain), n_2 (4%-6% engineering strain) and uniform elongation (UE) of annealed steels with standard galvanizing (F1) and supercool processing (G1)

Designation	n_1	n_2	UE (%)*	Designation	n_1	n_2	UE (%)*
5M7J, F1	0.591	0.134	8.59	5M7J, G1	0.538	0.140	8.82
5M8J, F1	0.662	0.110	7.48	5M8J, G1	0.807	0.097	7.51
6M7J, F1	0.643	0.122	8.14	6M7J, G1	0.588	0.127	8.94
6M8J, F1	0.640	0.108	7.69	6M8J, G1	0.872	0.097	7.69
5N7J, F1	0.729	0.156	8.72	5N7J, G1	0.488	0.167	3.83
5N8J, F1	0.600	0.105	7.95	5N8J, G1	0.471	0.121	8.54
6N7J, F1	0.425	0.136	8.54	6N7J, G1	0.433	0.120	7.77
6N8J, F1	0.676	0.120	9.16	6N8J, G1	0.475	0.118	8.03

*UE (%) represents the uniform elongation with 10 mm (0.4 in) gage length.

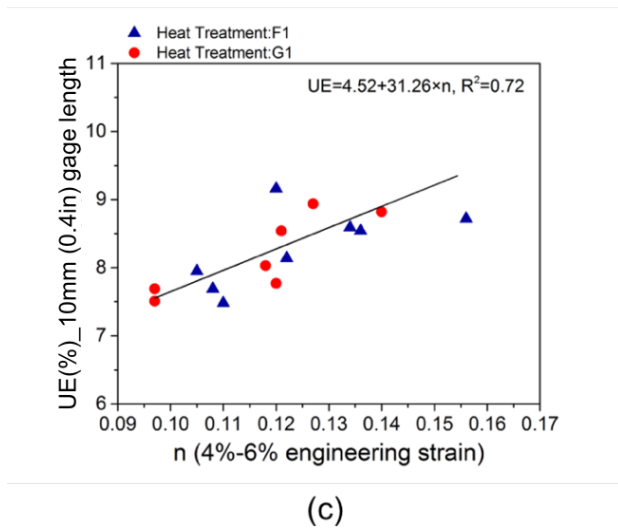
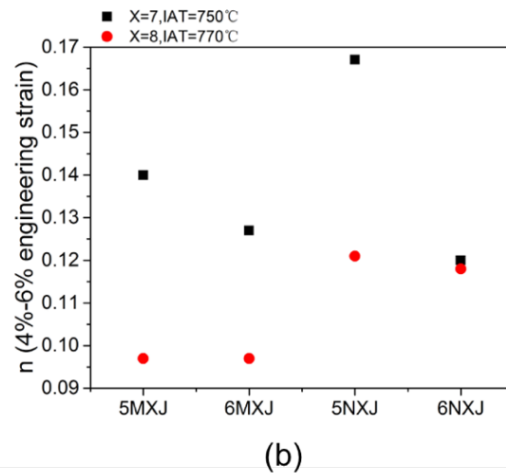
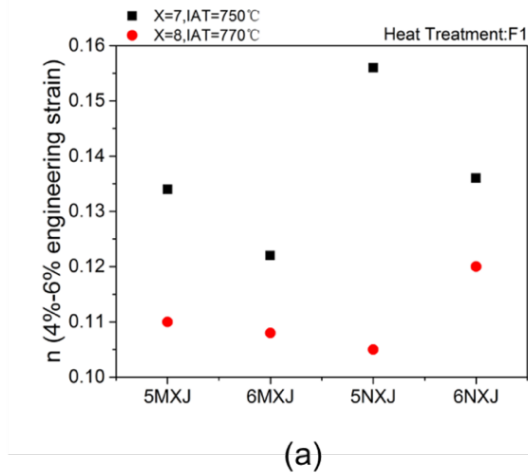


Figure 5.11 a) n values at 4%-6% engineering strain of steels annealed by standard galvanizing (F1); b) n values at 4%-6% engineering strain of steels annealed by supercool processing (G1); c) the relationship between uniform elongations (10 mm gage length) and n values, and the fitting curve of these data is a positive straight line, of which the linear equation is $UE=4.52+31.26 \times n$, with $R^2=0.72$.

5.2.2 Microstructures

Figure 5.12 compares SEM microstructures of 5N7J (CT=500°C, CR=72%, AT=750°C, IHT=15s and F1) and 5N8J (CT=500°C, CR=72%, AT=770°C, IHT=15s and F1). These two steels have the same pre-annealing condition, isothermal holding time at 460°C and annealing path, but with different annealing temperature. The higher annealing temperature coarsens the ferrite grain sizes and increases the volume fraction of martensite (V_m of 5N7J=48.2%, V_m of 5N8J=54.1%), since, according to the level rule, more austenite is formed during annealing at higher annealing temperatures, and, after cooling, a larger amount of martensite would be found in the final microstructures. SEM microstructures of 5M7J (CT=500°C, CR=58%, AT=750°C, IHT=15s and F1) and 5M8J (CT=500°C, CR=58%, AT=770°C, IHT=15s and F1) are shown in Figure 5.13. The volume fraction of martensite of 5M8J (V_m of 5M8J=50.7%) is less than that of 5M7J (V_m of 5M7J=52.9%).

Figure 5.14 compares SEM microstructures of 5N8J (CT=500°C, CR=72%, AT=770°C, IHT=15s and F1) and 5N8K (CT=500°C, CR=72%, AT=770°C, IHT=30s and F1). These two steels have the same pre-annealing condition, annealing temperature and annealing path but with different soaking times at zinc pot temperature. The DP steels with long soaking time (30s) have coarser ferrite grains than those with short isothermal holding time (15s). The martensite volume fraction of 5N8K is slightly less than that of 5N8J (V_m of 5N8J=54.1%, V_m of 5N8K=53.1%). SEM microstructures of 5M8J (CT=500°C, CR=58%, AT=770°C, IHT=15s and F1) and 5M8K (CT=500°C, CR=58%, AT=770°C, IHT=30s and F1) are given in Figure 5.15.

The effect of coiling temperatures on the microstructures of dual-phase steels can be explained by Figure 5.16. It compares the SEM microstructures of 5N7J (CT=500°C, CR=72%, AT=750°C, IHT=15s and F1) and 6N7J (CT=650°C, CR=72%, AT=750°C, IHT=15s), F1(Standard Galvanizing), which illustrates that DP steels with low coiling temperature have more refined microstructures than the ones with high coiling temperature and that the increase in tensile strength is mainly attributed to these refined microstructures.

Moreover, cold reduction has a significant role in final microstructures of dual phase steels. SEM microstructures of 5N8J (CT=500°C, CR=72%, AT=770°C, IHT=15s and F1) and 5M8J (CT=500°C, CR=58%, AT=770°C, IHT=15s and F1) are shown in Figure 5.17. The higher cold reduction leads to finer ferrite grains and martensite islands. It also helps to avoid severe martensite bands which appear in the final microstructures of steels with lower cold reduction. In addition, the higher cold reduction results in high martensite volume fraction, which helps to improve tensile strength of DP steels (V_m of 5N8J=61.5% and V_m of 5M8J=56.0%).

Figure 5.18 compares SEM microstructures of 5N8J (CT=500°C, CR=72%, AT=770°C, IHT=15s and F1) and 5N8J (CT=500°C, CR=72%, AT=770°C, IHT=15s and G1). These two steels were annealed by different annealing paths. In the final microstructure of the steel annealed by standard galvanizing, there are two phases, ferrite and martensite. In terms of the steels annealed by supercool processing, three phases could be observed in final microstructure, ferrite, martensite and tempered martensite. In the supercool processing, the intercritically formed austenite transformed to martensite, which would be tempered at zinc pot temperature [1]. The retained austenite transformed to fresh martensite, as the steel was cooled from 460°C to room temperature. The limited amount of fresh martensite in the final microstructures is the main reason for the low tensile strength.

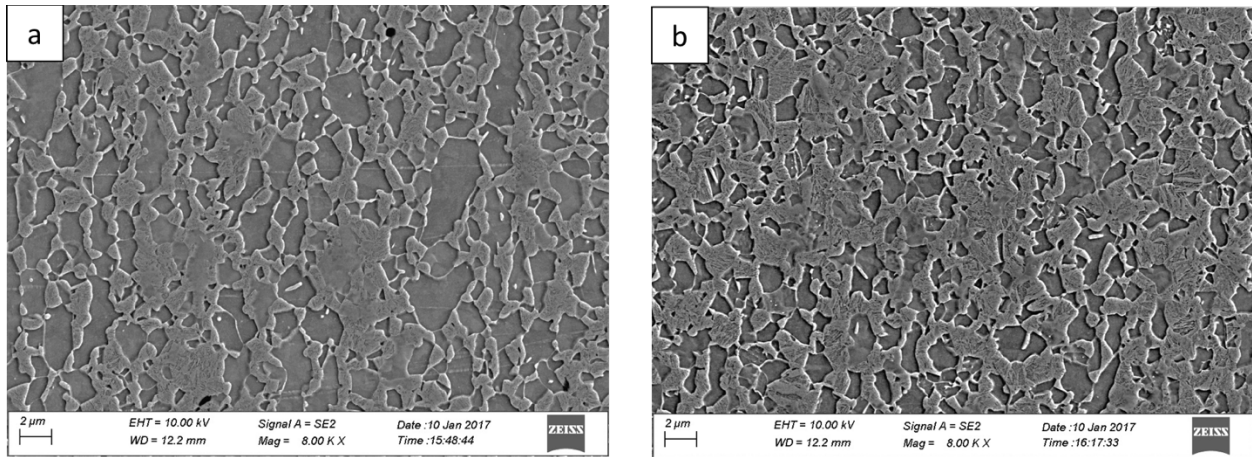


Figure 5.12 SEM microstructures of annealed steels with different intercritical annealing temperatures (IAT), a) 5N7J (CT=500°C, CR=72%, AT=750°C, IHT=15s), F1(Standard Galvanizing), b) 5N8J (CT=500°C, CR=72%, AT=770°C, IHT=15s), F1(Standard Galvanizing)

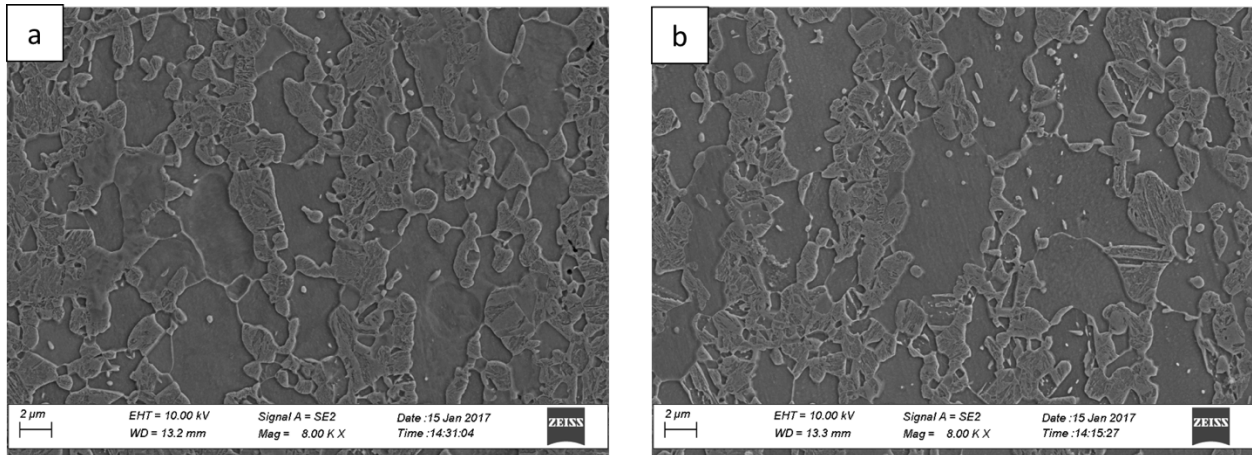


Figure 5.13 SEM microstructures of annealed steels with different intercritical annealing temperatures (IAT), a) 5M7J (CT=500°C, CR=58%, AT=750°C, IHT=15s), F1(Standard Galvanizing), b) 5M8J (CT=500°C, CR=58%, AT=770°C, IHT=15s), F1(Standard Galvanizing)

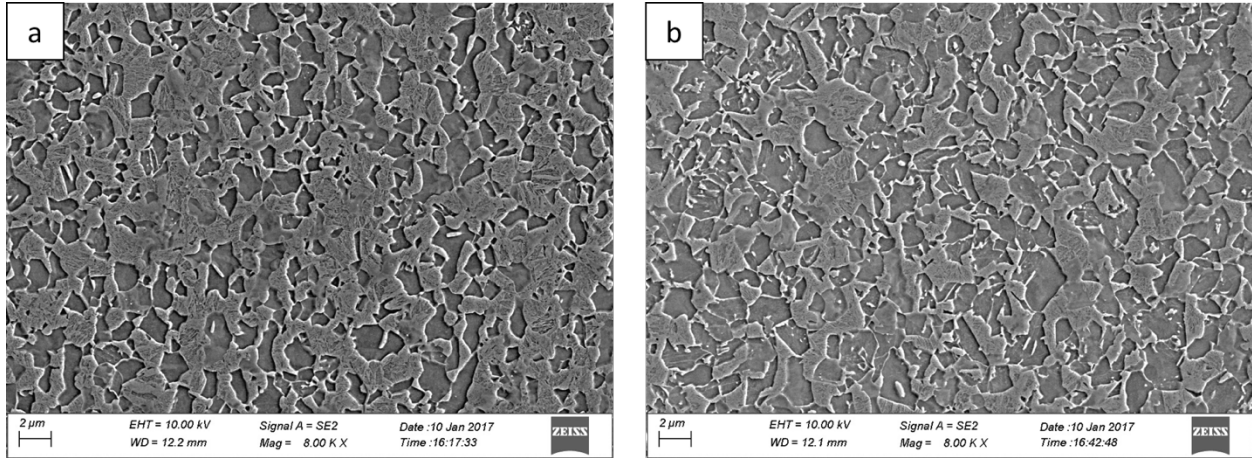


Figure 5.14 SEM microstructures of annealed steels with different isothermal holding time (IHT) at zinc pot temperature, a) 5N8J (CT=500°C, CR=72%, AT=770°C, IHT=15s), F1(Standard Galvanizing), b) 5N8K (CT=500°C, CR=72%, AT=770°C, IHT=30s), F1(Standard Galvanizing)

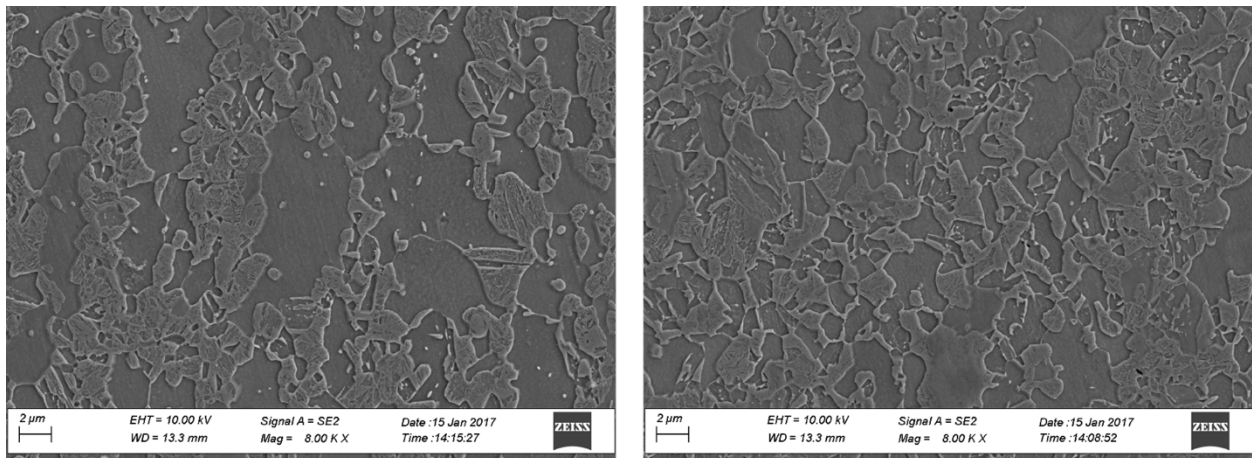


Figure 5.15 SEM microstructures of annealed steels with different isothermal holding time (IHT) at zinc pot temperature, a) 5M8J (CT=500°C, CR=58%, AT=770°C, IHT=15s), F1(Standard Galvanizing), b) 5M8K (CT=500°C, CR=58%, AT=770°C, IHT=30s), F1(Standard Galvanizing)

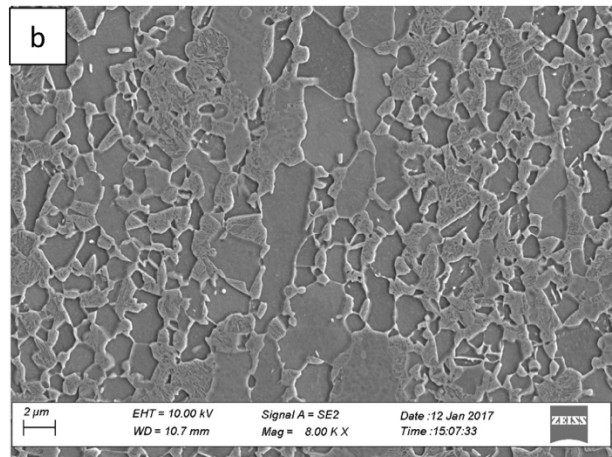
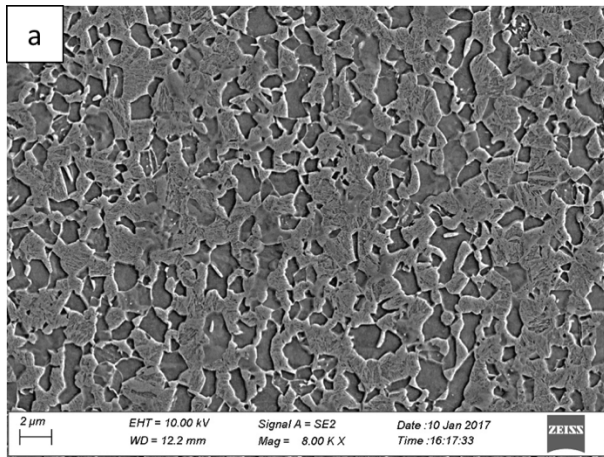


Figure 5.16 SEM microstructures of annealed steels with different coiling temperatures, a) 5N7J (CT=500°C, CR=72%, AT=750°C, IHT=15s), F1(Standard Galvanizing), b) 6N7J (CT=650°C, CR=72%, AT=750°C, IHT=15s), F1(Standard Galvanizing)

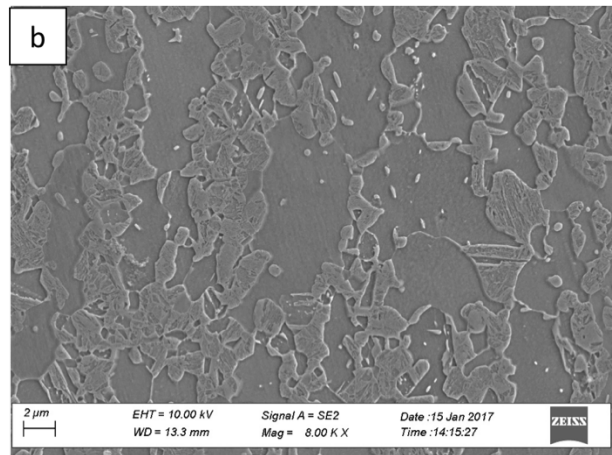
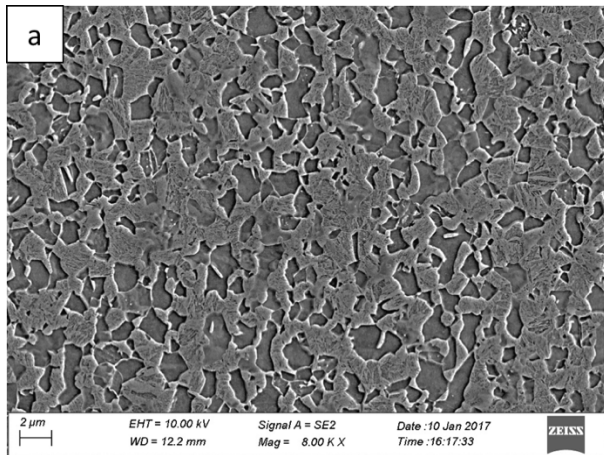


Figure 5.17 SEM microstructures of annealed steels with different cold reduction, a) 5N8J (CT=500°C, CR=72%, AT=770°C, IHT=15s), F1(Standard Galvanizing), b) 5M8J (CT=500°C, CR=58%, AT=770°C, IHT=15s), F1(Standard Galvanizing)

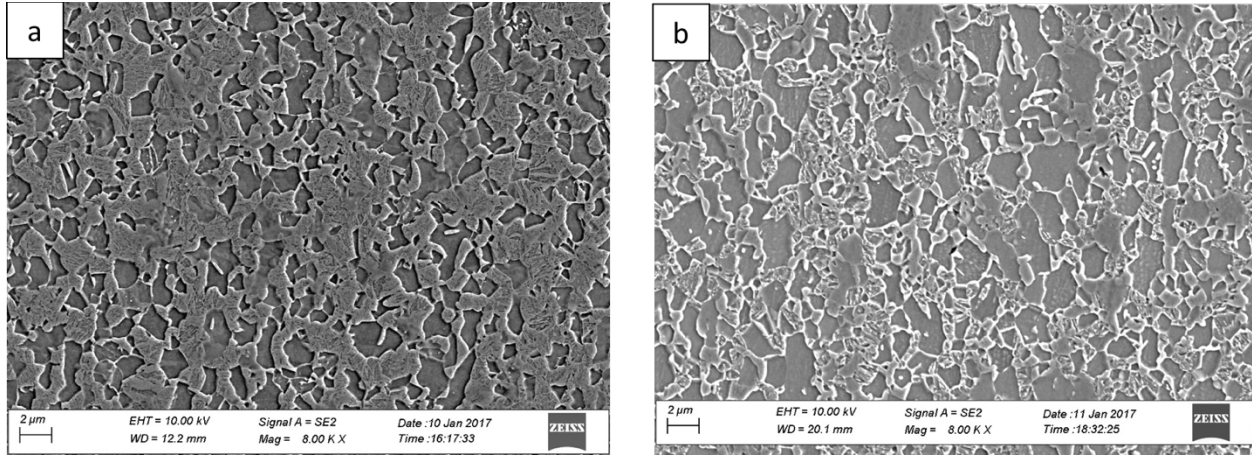


Figure 5.18 SEM microstructures of annealed steels with different annealing paths, a) 5N8J (CT=500°C, CR=72%, AT=770°C, IHT=15s), F1(Standard Galvanizing), b) 5N8J (CT=500°C, CR=72%, AT=770°C, IHT=15s), G1(Supercool processing)

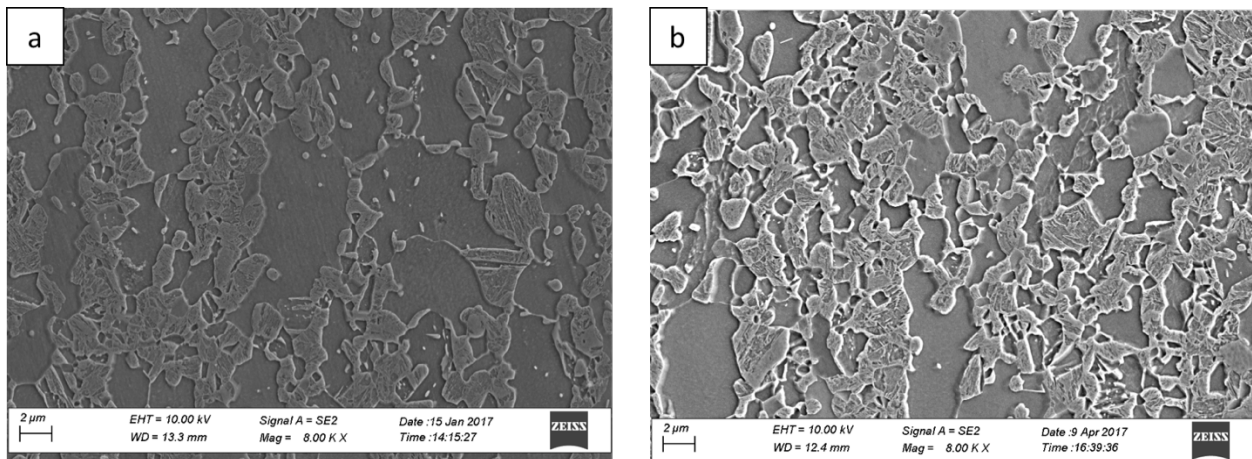


Figure 5.19 SEM microstructures of annealed steels with different annealing paths, a) 5M8J (CT=500°C, CR=58%, AT=770°C, IHT=15s), F1(Standard Galvanizing), b) 5M8J (CT=500°C, CR=58%, AT=770°C, IHT=15s), G1(Supercool processing)

The ferrite grain sizes and volume fraction of martensite of different specimens annealed by standard galvanizing (F1) and supercool (G1) are given in Table 5.9 and Table 5.10. The relationship between strength and volume fraction of martensite of annealed steels are plotted in

Figure 5.20. The UTS of dual phase steels containing 0.10 wt.% carbon is also included in Figure 5.20. From Figure 2.4 in Section 2, that figure was plotted from Davies' data. In that figure, there were two straight lines; the upper one illustrated the relationship between the tensile strength and volume fraction of martensite, expressed by Equation (5-5), and the lower one represented that yield strength and volume fraction of martensite had a positive linear relation, expressed by Equation (5-6).

$$\text{UTS}=365+16.3\times V_m \quad (5-5)$$

$$\text{YS}=103+11.1\times V_m \quad (5-6)$$

They suggested that the increasing volume fraction of martensite improved both tensile strengths and yield strengths. The line with Equation (5-5) is also shown in Figure 5.20. All the tensile strengths of dual phase with 0.15wt.% carbon or 0.10wt.% carbon increase with the increasing of the volume fraction of martensite. The relationship between tensile strengths of dual-phase with 0.15 wt.% carbon can be expressed by Equation (5-7) with $R^2=0.82$. While, for the data of dual-phase steels containing 0.10 wt.%, the relation between UTS and V can be expressed by Equation (5-8) with $R^2=0.57$.

$$\text{UTS}=708.95+10.64\times V_m \quad (5-7)$$

$$\text{UTS}=795+6.08\times V_m \quad (5-8)$$

In Figure 5.20, the tensile strengths of DP steels with 0.15 wt.% carbon are all above 1200MPa with V_m ranging from 45% to 55%; while the UTS of DP steels containing 0.1 wt.% carbon are from 900MPa to 1000MPa and the V_m are from 20% to 30%. These indicate, the volume fraction of martensite plays an important role in the difference of tensile strengths. In terms of dots of tensile strength in this study, most of these data are above the tensile line which was proposed by

Davies. The tensile strength might be attributed to the grain refinement, since the average ferrite grain sizes in this research are very small ($d=1-2\ \mu\text{m}$) and the addition of vanadium can have a significant effect on ferrite grain refinement. It also illustrates that tensile strength is grain size dependent.

Figure 5.21 shows the distribution of ferrite grain sizes with two different cold reductions; 6M7K, F1 (CR=58%) and 6N7K, F1 (CR=72%). The distribution of ferrite grain sizes with high cold reduction can be expressed by one Gaussian curve with one peak and the standard deviation is small, indicating the ferrite grains with high cold reduction are uniform and refined. The distribution of ferrite grain sizes with low cold reduction can be fitted by two Gaussian curves with two peaks and the standard deviation is larger than the former one. This bimodal distribution represents that ferrite grains of low cold reduction are not uniform; some of them are new recrystallized ferrite and some are non-recrystallized, which indicate that cold reduction influences the distribution of ferrite grain sizes of dual phase steels. Because the high cold reduction introduces a high density of lattice defects, generating more nucleation sites for the recrystallization of ferrite and the formation of austenite [1]. During annealing, these nucleation sites ensure the uniformity and refinement of those grains. In contrast, the low cold reduction results in low stored energy, creating relatively insufficient driving force for the recrystallization of ferrite and formation of austenite, and as a result the ferrite grains are nonuniform and coarse.

Table 5.9 Ferrite grain sizes (d_F), volume fraction of martensite (V_m) and retained austenite(V_{γ_r}) of steels annealed by standard galvanizing (F1)

Designation	$d_F(\mu\text{m})$	$V_m(\%)$	$V_{\gamma_r}(\%)$	Designation	$d_F(\mu\text{m})$	$V_m(\%)$	$V_{\gamma_r}(\%)$
5M7J, F1	1.66±1.39	52.9	0.20	5N7J, F1	1.33±0.85	48.2	0.32
5M7K, F1	1.71±1.13	53.2	0.63	5N7K, F1	1.37±0.73	50.4	0.37
5M8J, F1	1.83±1.09	51.0	1.16	5N8J, F1	1.40±0.77	54.1	2.52
5M8K, F1	1.89±1.05	50.7	1.52	5N8K, F1	1.59±0.71	53.1	3.32
6M7J, F1	1.84±0.91	46.2	0.14	6N7J, F1	1.35±0.96	47.5	0.21
6M7K, F1	2.44±1.77	43.1	0.47	6N7K, F1	1.21±0.74	50.3	0.38
6M8J, F1	2.14±1.33	53.2	0.77	6N8J, F1	1.40±0.89	52.8	1.49
6M8K, F1	2.31±1.63	51.8	1.93	6N8K, F1	1.45±0.74	52.3	3.00

Table 5.10 Ferrite grain sizes (d_F), volume fraction of martensite (V_m), tempered martensite (V_{TM}) and retained austenite(V_{γ_r}) of steels annealed by supercool processing (G1)

Designation	$d_F(\mu\text{m})$	$V_m(\%)$	$V_{TM}(\%)$	$V_{\gamma_r}(\%)$	Designation	$d_F(\mu\text{m})$	$V_m(\%)$	$V_{TM}(\%)$	$V_{\gamma_r}(\%)$
5M7J, G1	1.95±1.24	4.9	50.9	0.87	5N7J, G1	1.28±0.82	13.7	51.3	0.27
5M7K, G1	1.99±1.48	5.7	50.7	0.94	5N7K, G1	1.35±0.73	13.2	49.5	0.27
5M8J, G1	2.24±1.49	8.6	53.4	1.44	5N8J, G1	1.37±0.54	12.7	59.7	2.42
5M8K, G1	1.53±1.06	7.6	52.7	1.20	5N8K, G1	1.38±0.58	13.9	58.9	3.20
6M7J, G1	2.00±1.36	9.3	50.4	0.62	6N7J, G1	1.21±0.77	13.2	49.1	0.24
6M7K, G1	2.14±1.18	10.4	48.4	0.73	6N7K, G1	1.27±0.64	14.5	47.3	0.26
6M8J, G1	1.99±1.27	8.4	51.5	2.10	6N8J, G1	1.20±0.59	11.4	57.1	1.37
6M8K, G1	1.80±1.01	7.7	49.1	-	6N8K, G1	1.21±0.69	13.4	55.9	1.87

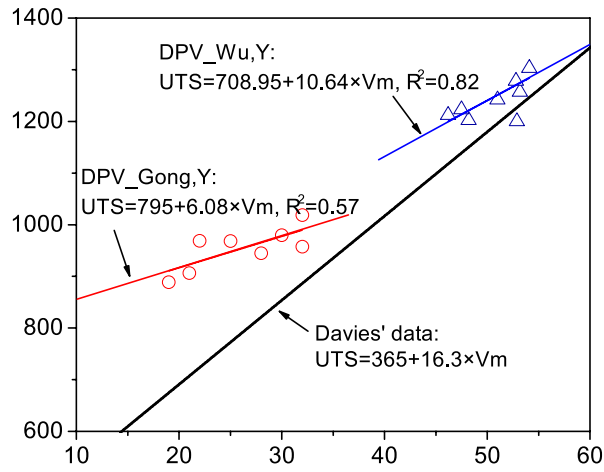


Figure 5.20 The relationship between stress and volume fraction of martensite of steels annealed by standard galvanizing (F1) in this research, the upper solid line illustrates the relationship between UTS and V_m and the lower solid line represents YS and V_m have a linear relation, proposed by Davies.

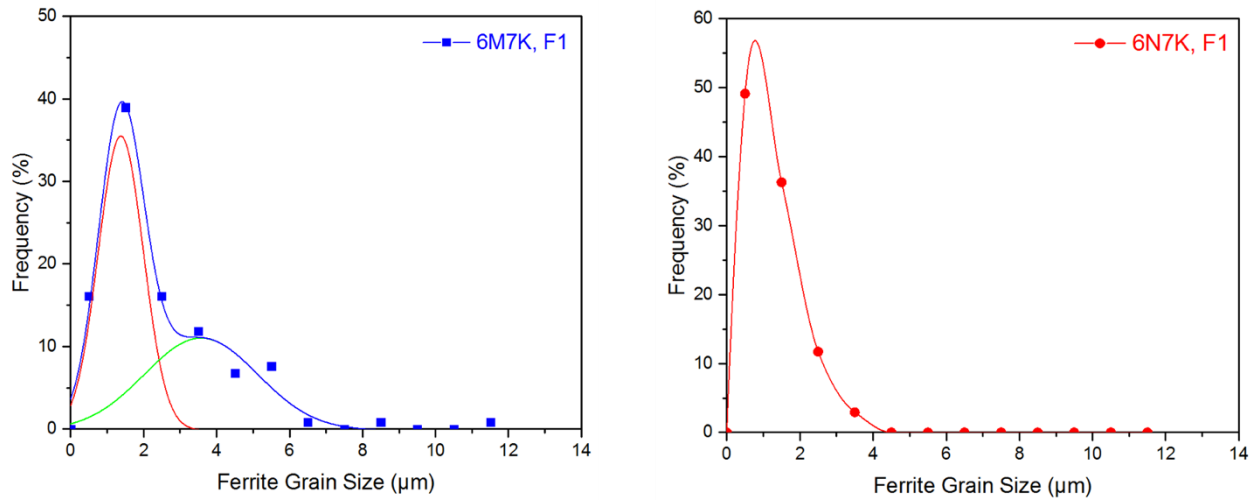


Figure 5.21 Distribution of ferrite grain sizes of 6M7K (CR=58%) and 6N7K (CR=72%) with standard galvanizing (F1)

5.2.3 Nanohardness of ferrite and martensite

To investigate the relationship of martensite volume fraction and martensite hardness and the effect of martensite volume fraction and martensite hardness on tensile strength and uniform elongations of dual phase steels annealed by standard galvanizing (F1), nanohardness tests were applied by Hysitron TriboIndenter. Twenty-five nanoindentations were performed on each polished sample, with a pattern of 5 rows \times 5 columns. The spacing of each indenter was 4 μm .

All the SEM images of nanoindenters as well as microstructures of tested samples are shown in Figure 5.22-5.25. In each SEM image, the nanoindenters circled by green solid circles represent the indenters within the martensite; the ones surrounded by red dashed circles show the indenters within the ferrite; and those marked by white dashed circles indicate the indenters are within the mixed microstructures (ferrite + martensite regions). The nanohardness of both ferrite and martensite of each steel are given in the Table 5.11. Figure 5.22 a) and Figure 5.23 a) compare the ferrite nanohardness of 5M7J (CT=500°C, CR=58%, IAT=750°C) and 6M7J (CT=650°C, CR=58%, IAT=750°C), and ferrite nanohardness of higher coiling temperature is slightly higher than that of lower coiling temperature (NHN_F of 6M7J=3.56 \pm 0.19 GPa, NHN_F of 5M7J=3.50 \pm 0.15 GPa). Similarly, in Figure 5.22 b) and Figure 5.23 b), when the cold reduction is 58% and annealing temperature is 770°C, NHN_F of 6M8J=3.47 \pm 0.19 GPa and NHN_F of 5M8J=3.45 \pm 0.15 GPa, illustrating that, with low cold reduction (58%), the higher coiling temperature could result in higher tensile strength, even though the DP steels have coarser microstructures. Since with the addition of vanadium, the precipitates in the ferrite help to increase the tensile strength. Figure 5.24 a) and Figure 5.25 a) compare the ferrite nanohardness of 5N7J (CT=500°C, CR=72%, IAT=750°C) and 6N7J (CT=650°C, CR=72%, IAT=750°C), and the

ferrite hardness of 5N7J is higher than that of 6N7J). Because high cold reduction provides the annealed steels with refined microstructures and high Sv, this increases the strength and hardness of the ferrite.

Figure 5.26 shows the relationship between nanohardness of martensite (NHN_m) and volume fraction of martensite (V_m) of steels annealed by standard galvanizing (F1) and the fitting curve of these data is a negative straight line, expressed by Equation (5-9) with $R^2=0.54$. Figure 5.26 illustrates, with a constant carbon content, increasing the martensite volume fraction reduces the martensite hardness. However, from the Figure 5.26, tensile strength increases with the improvement of martensite volume fraction, and both martensite and ferrite with vanadium carbides precipitates help to raise the UTS of annealed specimens.

$$NHN_m = 21.56 - 0.256 \times V_m \quad (5-9)$$

Figure 5.27 shows the HER (predicted from RA data) vs ΔNHN ($= NHM_M - NHN_F$). Increasing the difference in nanohardness between martensite and ferrite decreases the hole expansion ratio. This also explains the reason why hole expansion ratios of dual-phase steels annealed by standard galvanizing are lower than those of dual-phase steels annealed by supercool processing. Martensite is replaced by tempered martensite, and compared with fresh martensite, tempered martensite is softer, thereby decreasing the HER.

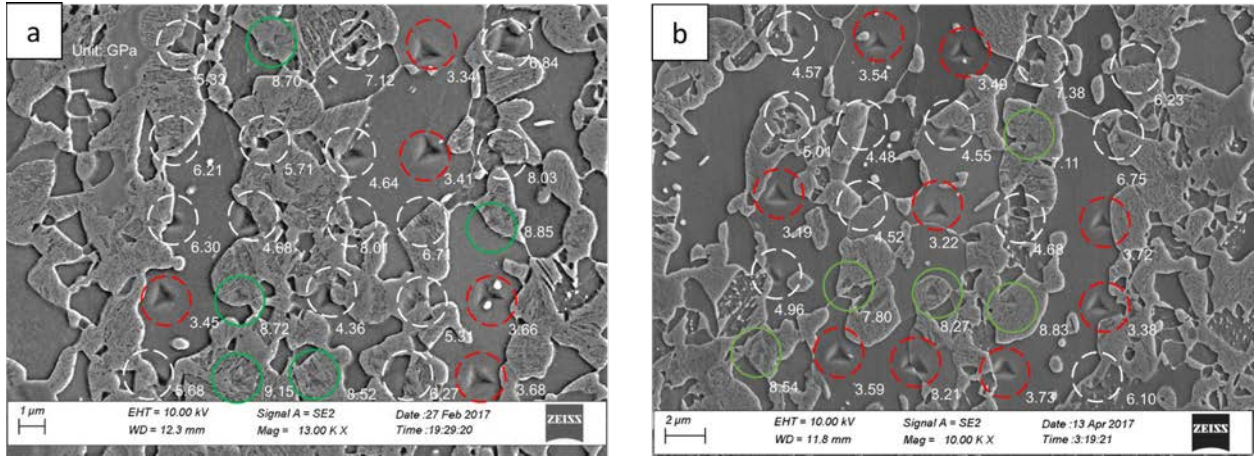


Figure 5.22 SEM images of nanoindenters, a) 5M7J (CT=500°C, CR=58%, IAT=750°C), and b) 5M8J (CT=500°C, CR=58%, IAT=770)

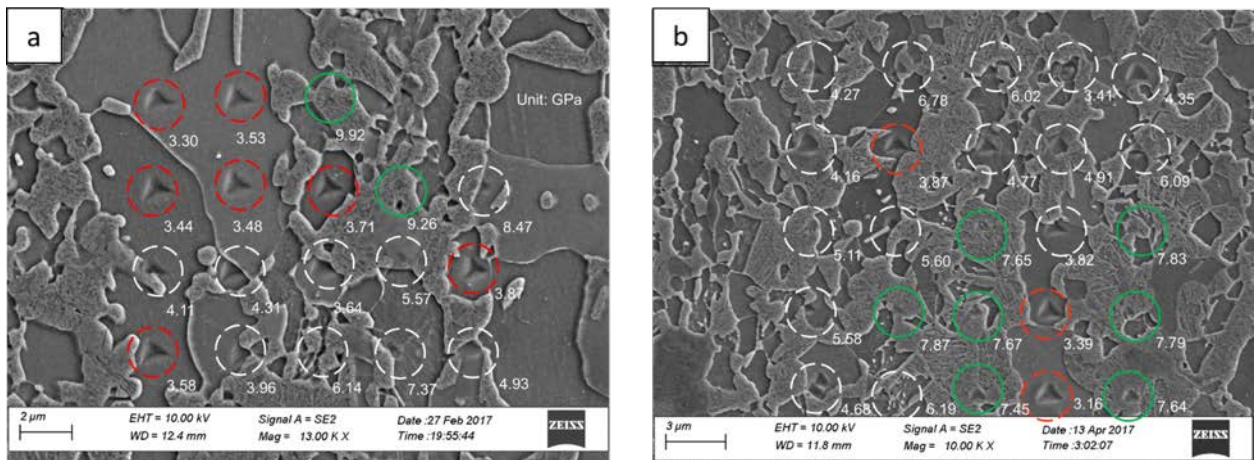


Figure 5.23 SEM images of nanoindenters a) 6M7J (CT=650°C, CR=58%, IAT=750°C), and b) 6M8J (CT=650°C, CR=58%, IAT=770°C)

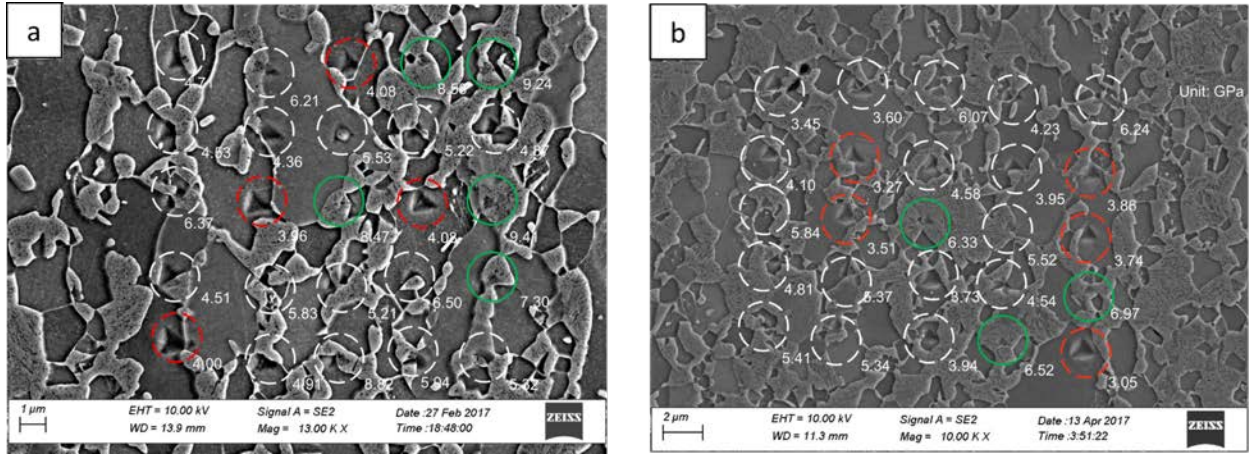


Figure 5.24 SEM images of nanoindenters a) 5N7J (CT=500°C, CR=72%, IAT=750°C), and b) 5N8J (CT=500°C, CR=72%, IAT=770°C)

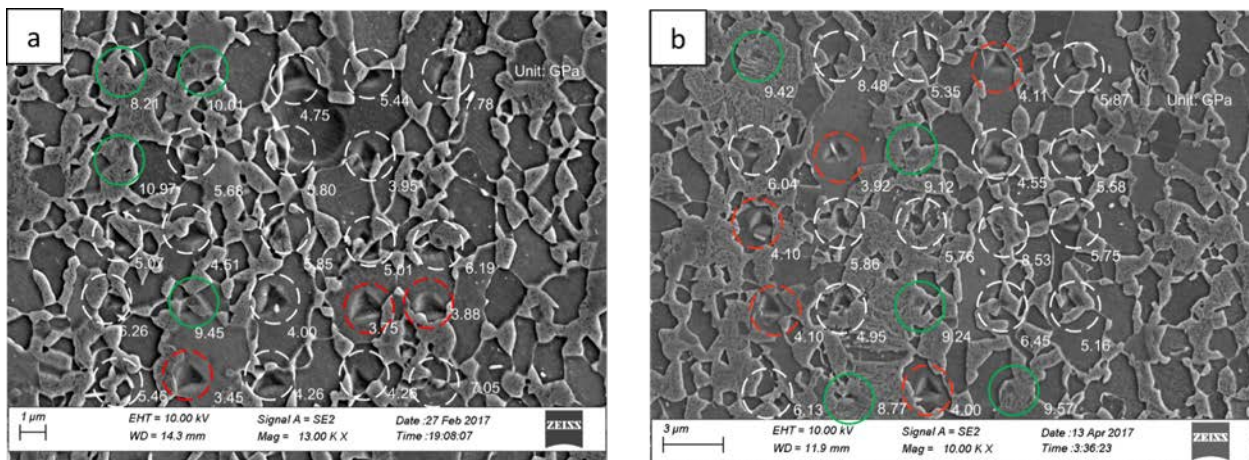


Figure 5.25 SEM images of nanoindenters a) 6N7J (CT=650°C, CR=72%, IAT=750°C), and b) 6N8J (CT=650°C, CR=72%, IAT=770°C)

Table 5.11 Nanohardness (GPa) of ferrite and martensite of dual-phase steels annealed by standard galvanizing (F1)

Designation	5M7J	5M8J	6M7J	6M8J	5N7J	5N8J	6N7J	6N8J
NHN of α	3.50±0.15	3.45±0.24	3.56±0.19	3.47±0.36	4.03±0.06	3.49±0.33	3.69±0.22	4.05±0.08
NHN of α'	8.79±0.23	8.07±0.77	9.59±0.47	7.67±0.14	8.98±0.42	6.60±0.33	9.66±1.55	9.22±0.30

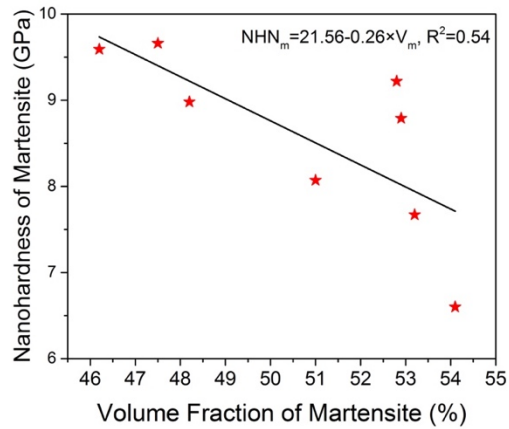


Figure 5.26 The relationship between nanoindentation hardness of martensite (NHN_m) and volume fraction of martensite (V_m) of steels annealed by standard galvanizing (F1).

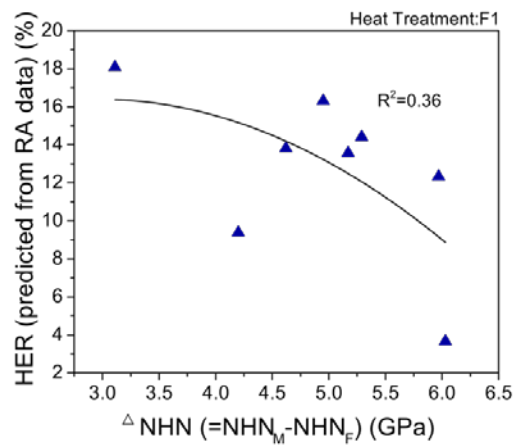


Figure 5.27 The relationship between hole expansion ratio and nanoindentation hardness of difference of martensite and ferrite

5.2.4 Measurement of retained austenite

The volume fraction of retained austenite can be expressed by Equation (5-10).

$$f_Y = 1 - \frac{M_s(c)}{M_s(f)} \quad (5-10)$$

where, f_γ is the volume fraction of retained austenite, $M_s(c)$ is the saturation magnetization of samples containing austenite, $M_s(f)$ is the saturation magnetization of samples without austenite [1]. The saturation magnetization can be obtained from the magnetic curve and the volume fraction of retained austenite. Taking dual-phase steel 5M8K, G1 as an example, the sample was tested to obtain the $M_s(c)$; afterwards, the sample was inserted into liquid nitrogen to eliminate retained austenite and then the sample was tested to obtain the $M_s(f)$. The Moment/Mass vs Magnetic Field curves of 5M8K, G1 with and without retained austenite are shown in Figure 5.28. According to Equation (5-10), the volume fraction of retained austenite should be 3.32%. The volume fraction of retained austenite of 16 dual-phase steels are given in Table 5.12.

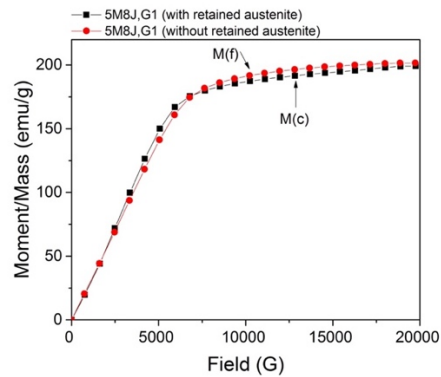


Figure 5.28 The Moment/Mass vs Field of dual-phase steel 5M8K, G1

Table 5.12 Volume fraction of retained austenite ($V_{\gamma'}$) of dual-phase steels annealed by standard galvanizing (F1) and supercool processing (G1)

Designation	$V_{\gamma'}$ (%)						
5M7J, F1	0.20	5N7J, F1	0.32	5M7J, G1	0.87	5N7J, F1	0.27
5M8J, F1	1.16	5N8J, F1	2.52	5M8J, G1	1.44	5N8J, F1	2.42
6M7J, F1	0.14	6N7J, F1	0.21	6M7J, G1	0.62	6N7J, F1	0.24
6M8J, F1	0.77	6N8J, F1	1.49	6M8J, G1	2.10	6N8J, F1	1.37

The results showed that retained austenite volume fraction ($V_{\gamma'}$) can be controlled by different factors. From Figure 5.29, the retained austenite volume fraction at 770°C is higher than that at 750°C, indicating that increasing temperature improves the retained austenite volume fraction. In addition, when compared with the volume fraction of retained austenite ($V_{\gamma'}$) of dual phase steels annealed by standard galvanizing, $V_{\gamma'}$ of steels annealed by supercool processing do not have much difference. This might be attributed to the supercool temperature of 200°C in this study. The supercool temperature was too low, near the M_s temperature, so not too much retained austenite would be formed.

Figure 5.30 (a) and (b) represent the relationship between HER (predicted from RA data) or RA and the volume fraction of retained austenite ($V_{\gamma'}$). In Figure 5.30 (a), HER (predicted from RA data) and $V_{\gamma'}$ have a linear relationship, which can be expressed by Equation (5-11) and $R^2=0.59$. Figure 5.30 (b) shows that reduction in area can be expressed by the Equation (5-12) regarding $V_{\gamma'}$ with $R^2=0.57$. Both equations indicate increasing the volume fraction of retained austenite, HER and RA would increase.

$$\text{HER}=5.84 \times V_{\gamma'} + 11.38 \quad (5-11)$$

$$\text{RA}=4.71 \times V_{\gamma'} + 18.05 \quad (5-12)$$

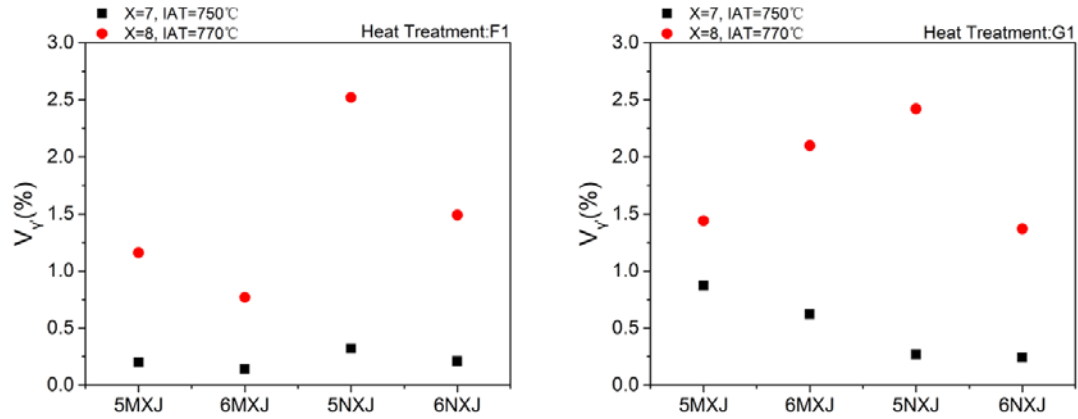


Figure 5.29 Volume fraction of retained austenite vs annealing temperature of dual-phase steels annealed by standard galvanizing (F1) and supercool processing (G1)

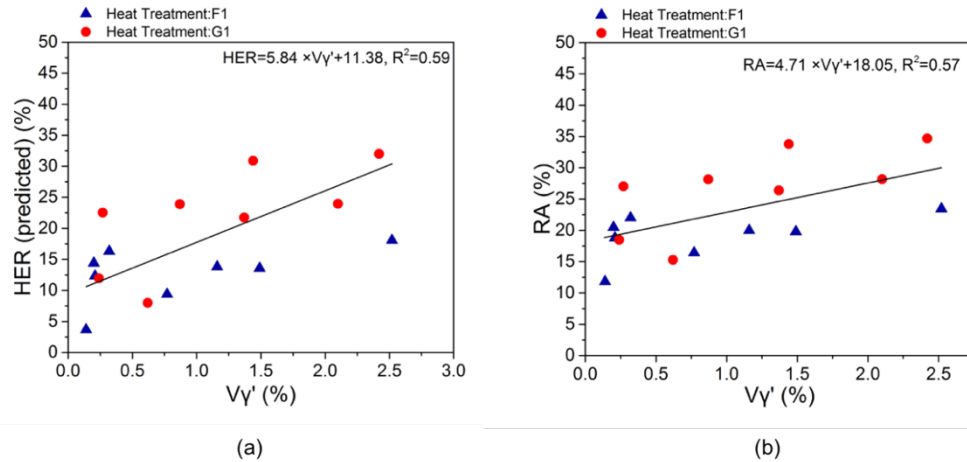


Figure 5.30 The relationship between HER (predicted from RA data) or RA and volume fraction of retained austenite ($V_{\gamma'}$). a) HER (predicted) vs $V_{\gamma'}$, with the fitting curve of $HER=5.84 \times V_{\gamma'} + 11.38$, $R^2=0.59$, b) $RA=4.71 \times V_{\gamma'} + 18.05$,

$$R^2=0.57$$

6.0 DISCUSSION

The present study was designed to find an optimized way to produce dual-phase steels with ultra-high strength, good global ductility and excellent local ductility. The product of $UTS \times TE$ could conform to the data of AHSS Generation III steels. The tensile results showed that the tensile strengths of dual phase steels annealed by standard galvanizing were all above 1200 MPa, which reached the minimum requirement of DP 1180. UTS of dual-phase steels annealed by supercool processing were above 1000 MPa, reaching the minimum requirement of DP 980. Although both series of dual-phase steels represented high-strength level, the difference in tensile strengths was obvious, which was mainly attributed to the final microstructures. According to microstructural analysis, the volume fraction of martensite of dual-phase steels annealed by standard galvanizing ranged from 45% to 55%; while, in terms of supercool processing, the final microstructures of dual-phase steels just consisted of 5% to 15% fresh martensite. Unlike standard galvanizing, during supercool processing, the steels were fast cooled from intercritical annealing temperature to supercool temperature (200°C), followed by up quenching to zinc pot temperature. The martensite transformed from intercritical austenite to tempered martensite, thereby reducing the tensile strength.

Apart from annealing path, this study also set out with the aim of assessing the effects of coiling temperatures, cold reductions and intercritical annealing temperatures on microstructures and properties of dual-phase steels.

The combination of low coiling temperature (500°C) and high cold reduction (72%) could have resulted in high tensile strengths of dual-phase steels. Because this combination would have high stored energy, the sum of the energy stored in the grain boundaries and the energy stored in the sub-grain boundaries in the ferrite grains [1]. High stored energy would provide more driving force for the austenite formation and ferrite recrystallization during intercritical annealing at a very short time (60s). After fast cooling, the intercritical austenite would transform into a large amount of martensite. Another important finding was that high annealing temperature (770°C) led to high tensile strength. From the level rule, higher intercritical annealing temperature increase the amount of austenite and after fast cooling, more martensite would be formed.

In terms of products of total elongation (TE) \times tensile strength (UTS), the aim of this study was to produce more dual-phase steels whose properties could conform to those of AHSS Generation III steels. Increasing the tensile strength, total elongation would be sacrificed. For the products of dual-phase steels annealed by standard galvanizing, most of them placed in the DP steels region and small part reached the minimum requirement of TRIP steels area. Regarding the steels annealed by supercool processing, most steels were near the boundary between DP steels and TRIP steels. The product of TE \times UTS of one steel was in the AHSS Generation III area with tensile strength of 1085 MPa.

In addition, hole expansion ratios (HER) vary with different annealing paths. HER of dual-phase steels annealed by supercool processing was higher than that of steels annealed by standard galvanizing, which affected by several factors. First, hard fresh martensite was replaced by soft tempered martensite, which decreased the difference of hardness between hard phase and soft phase [4]. From literature review, HER was affected by the difference (Δ NHN) in hardness of martensite and ferrite [72]. Nanohardness testing results indicated that HER decreased with the

increase of ΔNHN . Thus, formation of tempered martensite ensured the high HER. Furthermore, the enhanced HER ability could be attributed to the TRIP effect of retained austenite, which is the transformation from retained austenite into martensite upon straining [73]. TRIP effect could maintain higher strains or elongations of the microstructures before crack initiations or failure both during punching and hole expansion test [4], resulting in high HER value. According to microstructural analysis, compared with standard galvanizing, volume fraction of retained austenite of dual-phase steels annealed by supercool processing was little higher, lower than our expectations. This might be attributed to supercool temperature (200°C), which was too low to obtain enough retained austenite during fast cooling. Finally, the addition of vanadium helped to strengthen ferrite matrix, which lowered the hardness difference between ferrite and martensite, thereby increasing the HER of dual-phase steels annealed by both standard galvanizing and supercool processing.

Prior studies [27] [29] noted the importance of volume fraction of martensite on the tensile strength of dual-phase steels. From Davies' work, tensile strength was dependent on volume fraction of martensite, ferrite grain sizes and fine precipitates in ferrite matrix. The current study verified these facts; different pre-annealing and annealing conditions resulted in distinct volume fraction of martensite and both yield and tensile strengths increased with the increasing of martensite percent. However, these data were all above theoretical lines, which might be due to ferrite grain sizes. The addition of vanadium contributed to the grain refinement of polygonal ferrite (CT= 650°C) and acicular ferrite (CT= 500°C). A high density of polygonal ferrite nucleated on VN particles, which grew in the austenite during isothermal transformation or slow cooling at austenite region. Polygonal ferrite formed at coiling temperature of 650°C , while, acicular ferrite formed at coiling temperature of 500°C . The grain refinement effect of vanadium

enabled average ferrite grain sizes of dual-phase steels in this study ranged from 1-2 μm , thereby increasing the strengths.

The combination of nanohardness testing results and microstructural analysis indicated that at a given carbon content, increasing the volume fraction of martensite decreased the martensite hardness. This indicated that the tensile strength was independent on martensite hardness. As well, ferrite hardness remained stable even the ferrite volume fraction changed.

7.0 CONCLUSIONS

1. The combination of low coiling temperature (500°C), high cold reduction (72%) and high annealing temperature (770°C) enables dual-phase steels to have high tensile strength, reaching 1303 MPa. Low coiling temperature combined with high cold reduction (72%) would have high stored energy, the sum of the energy stored in the grain boundaries and the energy stored in the sub-grain boundaries in the ferrite grains. High stored energy would provide more driving force for the austenite formation and ferrite recrystallization during intercritical annealing at a very short time (60s). After fast cooling, the intercritical austenite would transform into a large amount of martensite. As well, high annealing temperature (770°C) leads to high tensile strength. From the level rule, higher intercritical annealing temperature increase the amount of austenite and after fast cooling, more martensite would be formed.

2. The combination of high coiling temperature (650°C), low cold reduction, high annealing temperature (770°C) and supercool processing can lead to the highest product of UTS × TE, conforming to AHSS Generation III steels, which is attributed to the largest volume fraction of retained austenite observed in the final microstructures.

3. The tensile strength of dual-phase steels in this study is mainly dependent on volume fraction of martensite as well as refined ferrite grains. From nanohardness results, at a given carbon content,

increasing the martensite volume fraction decreases the martensite hardness. Thus, tensile strength of dual-phase steels is not controlled by martensite strength.

4. The hole expansion ratio (HER) of dual phase steels annealed by supercool processing is larger than standard galvanizing, which can be explained by two factors: the difference of nanohardness (ΔNHN) between hard phase and soft phase and the volume fraction of retained austenite. HER increases with the reduction of ΔNHN . In supercool processing, hard fresh martensite was replaced by soft tempered martensite, thus decreasing ΔNHN and increasing HER. The volume fraction of retained austenite of dual phase steels annealed by supercool processing is larger than standard galvanizing. The volume fraction of retained austenite controls the HER, thus increasing the HER.

8.0 FUTURE WORK

Although the effects of coiling temperature, cold reduction, annealing temperature and annealing path on the microstructures and mechanical properties of dual-phase steels were investigated in this study, additional experiments need to be done.

First of all, the effect of vanadium on strength and HER still needs to be investigated in the future. New steel will be heated with the same chemical compositions of dual-phase steels in previous study (shown in Table 4.1), except for the vanadium content. The vanadium content would be reduced from 0.06wt% to 0. The microstructures and mechanical properties of v-free steels and v-bearing steels would be compared to reveal the effect of vanadium.

Secondly, in order to increase the ductility of ultra-high strength dual-phase steels, aluminum content will be increased to 0.4wt% or 0.8wt%. Because the ductility of dual-phase steels can be remarkably increased by the addition of aluminum.

In terms of annealing path, theoretically, steels annealed by supercool processing can have more volume fraction of retained austenite, leading to high HER. While, due to low supercool temperature, the amount of retained austenite was not expected. So, in the subsequent study, the supercool temperature would be increased to 250°C.

Last but not least, in order to find a more accurate relationship with HER and RA, more HER blanks would be machined and more HER tested would be implemented.

BIBLIOGRAPHY

- [1] Y. Gong, "The Mechanical Properties and Microstructures of Vanadium Bearing High Strength Dual Phase Steels Processed with Continuous Galvanizing Line Simulations," Ph.D. dissertation, Department of mechanical Engineering and Materials Science, University of Pittsburgh, Pittsburgh, PA, 2016.
- [2] M. S. Rashid, "High-Strength, Low-Alloy Steels," *Science*, vol. 208, no. 4446, pp. 862-869, 1980.
- [3] Y. Gong, M. Hua, J. Uusitalo and A. J. DeArdo, "Processing Factors That Influence the Microstructure and Properties of High-Strength Dual- Phase Steels Produced Using CGL Simulations," in *AISTech 2016 Proceedings*, Pittsburgh, 2016.
- [4] Y. Gong, M. Hua, J. Uusitalo and A. J. DeArdo, "Improving the Sheared-Edge Formability of High-Strength Dual-Phase Steel," in *AISTech 2016 Proceedings*, Pittsburgh, 2016.
- [5] Y. Gong, M. Hua, J. Uusitalo and A. J. DeArdo, "Effects of Thermomechanical processing and Vanadium Additions on Microstructures and Properties of High Strength Dual Phase Steels Processed with Continuous Galvanizing Line Simulations," in *Contributed Papers from Materials Science and Technology (MS&T) 2015*, Columbus, 2015.
- [6] V. L. de la Concepcion, H. N. Lorusso and H. G. Svoboda, "Effect of Carbon Content on Microstructure and Mechanical Properties of Dual Phase Steels," *Procedia Materials Science*, vol. 8, pp. 1047-1056, 2015.
- [7] Y. Toji, G. Miyamoto and D. Raabe, "Carbon partitioning during quenching and partitioning heat treatment accompanied by carbide precipitation," *Acta Materialia*, vol. 88, pp. 137-147, 2015.
- [8] M. S. Rashid, "Dual Phase Steels," *Annual Review of Materials Science*, no. 1, pp. 245-266, 08 1981.
- [9] G. R. Speich, "Physical Metallurgy of Dual-Phase Steels," in *Fundamental of Dual-Phase Steels*, Chicago, 1981.

- [10] E. J. Pavlina, C. J. Van Tyne and Y. H. Moon, "Influence of Production Method on the Properties of DualPhase Steel Tubes," *Journal of Engineering Materials and Technology*, vol. 132, no. 2, pp. 024501(1-10), 2010.
- [11] J. Huang, W. J. Poole and M. Militzer, "Austenite formation during intercritical annealing," *Metallurgical and Materials Transactions A*, vol. 35, no. 11, pp. 3363-3375, 2004.
- [12] H. Luo, J. Shi, C. Wang, W. Cao, X. Sun and H. Dong, "Experimental and Numerical Analysis on Formation of Stable Austenite During the Intercritical Annealing of 5Mn Steel," *Acta Materialia*, vol. 59, no. 10, pp. 4002-4014, 2011.
- [13] S. A. Etesami and M. H. Enayati, "Ferrite-Martensite Band Formation During the Intercritical Annealing," *Journal of Materials Engineering and Performance*, vol. 25, no. 2, pp. 349-358, 2016.
- [14] T. Tanaka, M. Nishida, K. Hashiguchi and T. Kato, "Formation and Properties of Ferrite Plus Martensite Dual-Phase Structures," in *Structure and Properties of Dual-Phase Steels*, 1979.
- [15] M. Sarwar, T. Manzoor, E. Ahmad and N. Hussain, "The role of connectivity of martensite on the tensile properties of a low alloy steel," *Materials & Design*, vol. 28, no. 6, pp. 1928-1933, 1 2007.
- [16] Y. Sakuma, D. K. Matlock and G. Krauss, "Intercritically annealed and isothermally transformed 0.15 Pct C steels containing 1.2 Pct Si-1.5 Pct Mn and 4 Pct Ni: Part I. transformation, microstructure, and room-temperature mechanical properties," *Metallurgical Transactions A*, vol. 23, no. 4, pp. 1221-1232, 1992.
- [17] Y. Gong, M. Hua, J. Uusitalo and A. J. DeArdo, "Improving Strength-Ductility Balance of High Strength Dual-Phase Steels by Addition of Vanadium," in *HSLA Steels 2015, Microalloying 2015 & Offshore Engineering Steels 2015: Conference Proceedings*, 2016.
- [18] D. K. Matlock, G. Krauss, L. F. Ramos and G. S. Huppi, "A Correlation of Processing Variables with Deformation Behavior of Dual-Phase Steels," in *Structure and Properties of Dual-Phase Steels*, 1979.
- [19] T. Furukawa and M. Tanino, "Structure Formation and Mechanical Properties of Intercritically Annealed or As-Hot-Rolled Dual-Phase Steels," in *Fundamentals of Dual-Phase Steels*, 1981.
- [20] N. Terao and A. Baugnet, "High-Manganese Dual-Phase Steels, Strengthened by Additional Elements (Cr, Ti, V, W)," *Journal of Material Science*, vol. 25, no. 2, pp. 848-858, 1990.

- [21] A. Chbihi, D. Barbier, L. Germain, A. Hazotte and M. Gouné, "Interactions between Ferrite Recrystallization and Austenite Formation in High-Strength Steels," *Journal of Materials Science*, vol. 49, no. 10, pp. 3608-3621, 2014.
- [22] M. Calcagnotto, D. Ponge and D. Raabe, "On the Effect of Manganese on Grain Size Stability and Hardenability in Ultrafine-Grained Ferrite/Martensite Dual-Phase Steels," *Metallurgical and Materials Transactions A*, vol. 43, no. 1, pp. 37-46, 2012.
- [23] K. HASHIGUCHI, M. NISHIDA, T. KATO and T. TANAKA, "Effects of Alloying Elements and Cooling Rate after Annealing on Mechanical Properties of Dual Phase Sheet Steel," in *KAWASAKI Steel Technical Report No.1*, 1980.
- [24] K.-C. Lin and C.-S. Lin, "Effect of Silicon in Dual Phase Steel on the Alloy Reaction in Continuous Hot-Dip Galvanizing and Galvannealing," *ISIJ International*, vol. 54, no. 10, pp. 2380-2384, 2014.
- [25] M. CAI, H. DING, Y. LEE, Z. TANG and J. ZHANG, "Effects of Si on Microstructural Evolution and Mechanical Properties of Hot-Rolled Ferrite and Bainite Dual-Phase Steels," *ISIJ International*, vol. 51, no. 3, pp. 476-481, 2011.
- [26] J. Drumond, O. Girina, J. F. da Silva Filho, N. Fonstein and C. A. Silva de Oliveira, "Effect of Silicon Content on the Microstructure and Mechanical Properties of Dual-Phase Steels," *Metallography, Microstructure, and Analysis*, vol. 1, no. 5, pp. 217-223, 2012.
- [27] R. G. Davies, "Influence of Silicon and Phosphorous on the Mechanical Properties of Both Ferrite and Dual-Phase Steels," *Metallurgical Transactions A*, vol. 10, no. 1, pp. 113-118, 1979.
- [28] C. Zhang, D. Cai, B. Liao and Y. Fan, "Using Direct Hot-Rolling Approach to Obtain Dual-Phase Weathering Steel Cu-P-Cr-Ni-Mo," *Journal of Materials Science*, vol. 45, no. 2, pp. 490-495, 2010.
- [29] R. G. Davies, "Influence of Martensite Composition and Content on the Properties of Dual Phase Steels," *Metallurgical Transactions A*, vol. 9, no. 5, pp. 671-679, 1978.
- [30] R. J. Glodowski, "A Review of Vanadium Microalloying in Hot Rolled Steel Sheet Products," in *International Seminar 2005 on Application Technologies of Vanadium in Flat-Rolled Steels*, 2005.
- [31] R. G. Davies, "The Deformation Behavior of A Vanadium-Strengthened Dual Phase Steel," *Metallurgical Transactions A*, vol. 9, no. 1, pp. 41-52, 1981.

- [32] A. R. Marder, "The Effect of Heat Treatment on the Properties and Structure of Molybdenum and Vanadium Dual-Phase Steels," *Metallurgical Transactions A*, vol. 12, no. 9, pp. 1569-1579, 1981.
- [33] A. Nakagawa, J. Y. Koo and G. Thomas, "Effect of Vanadium on Structure-Property Relations of Dual Phase Fe/ Mn/ Si/ 0.1C Steels," *Metallurgical Transactions A*, vol. 12, no. 11, pp. 1965-1972, 1981.
- [34] T. N. Baker, "Processes, Microstructure and Properties of Vanadium Microalloyed Steels," *Materials Science and Technology*, vol. 25, no. 9, pp. 1803-1107, 2009.
- [35] G. Rosenberg, I. Sinaiova and L. Juhar, "Effect of Microstructure on Mechanical Properties of Dual Phase Steels in the Presence of Stress Concentrators," *Materials Science and Engineering A*, vol. 582, pp. 347-358, 2013.
- [36] A. A. Sayed and S. Kheirandish, "Affect of the Tempering Temperature on the Microstructure and Mechanical Properties of Dual Phase Steels," *Materials Science and Engineering A*, vol. 532, pp. 21-25, 2012.
- [37] S. S. M. Tavares, P. D. Pedroza, J. R. Teodosio and T. Gurova, "Mechanical Properties of A Quenched and Tempered Dual Phase Steel," *Scripta Materialia*, vol. 40, no. 8, pp. 887-892, 1999.
- [38] Q. Lai, L. Brassart, O. Bouaziz, M. Goune, M. Verdier and G. Parry, "Influence of martensite volume fraction and hardness on the plastic behavior of dual-phase steels: Experiments and micromechanical modeling," *International Journal of Plasticity*, vol. 80, pp. 187-203, 2016.
- [39] I. Tamura, Y. Akao, Y. Yamaoha, M. Ozawa and S. Kanotoni, *Transactions of the Iron and Steel Institute of Japan*, vol. 13, pp. 283-292, 1973.
- [40] G. R. Speich and L. R. Miller, "Mechanical Properties of Ferrite Martensite Steels," in *Structure and Properties of Dual-Phase Steels*, 1979.
- [41] W. C. Leslie and R. J. Sober, "The Strength of Ferrite and of Martensite as Function of Composition, Temperature, and Strain Rate," *Transactions of the American Society of Metals*, vol. 60, pp. 459-487, 1967.
- [42] J. H. Hollomon and L. D. Jaffe, "Time-Temperature Relations in Tempering Steels," *Transactions of the Metallurgical Society of AIME*, vol. 162, pp. 223-249, 1945.
- [43] P. Movahed, S. Kolahgar, S. P. H. Marashi, M. Pournavari and N. Parvin, "The Effect of Intercritical Heat Treatment Temperature on the Tensile Properties and Work Hardening Behavior of Ferrite–Martensite Dual Phase Steel Sheets," *Materials Science & Engineering A*, vol. 518, pp. 1-6, 2009.

- [44] M. R. Akbarpour and A. Ekrami, "Effect of Ferrite Volume Fraction on Work Hardening Behavior of High Bainite Dual Phase (DP) Steels," *Materials Science & Engineering A*, vol. 477, pp. 306-310, 2008.
- [45] M. Pouranvari, "Work Hardening Behavior of Fe-0.1 C Dual Phase Steel," *BHM Berg-Und Hüttenmännische Monatshefte*, vol. 157, pp. 44-47, 2012.
- [46] S. N. Monteiro and R. E. Reed-Hill, "An empirical analysis of titanium stress-strain curves," *Metallurgical Transactions*, vol. 4, no. 4, pp. 1011-1015, 1973.
- [47] L. F. Ramos, D. K. Matlock and G. Krauss, "On the deformation behavior of dual-phase steels," *Metallurgical Transactions A*, vol. 10, no. 2, pp. 259-261, 1979.
- [48] M. Umemoto, K. Tsuchiya, Z. G. Liu and S. Sugimoto, "Tensile Stress-Strain Analysis of Single-Structure Steels," *Metallurgical and Materials Transactions A*, vol. 31, no. 7, pp. 1785-1794, 2000.
- [49] V. Colla, M. De Sanctis, A. Dimatteo, G. Lovicu, A. Solina and R. Valentini, "Strain Hardening Behavior of Dual-Phase Steels," *Metallurgical and Materials Transactions A*, vol. 40, no. 11, pp. 2557-2567, 2009.
- [50] D. Das and P. P. Chattopadhyay, "Influence of Martensite Morphology on the Work-Hardening Behavior of High Strength Ferrite–Martensite Dual-Phase Steel," *Journal of Materials Science*, vol. 44, pp. 2957-2965, 2009.
- [51] A. Bag, K. K. Ray and E. S. Dwarakadasa, "Influence of Martensite Content and Morphology on Tensile and Impact Properties of High-Martensite Dual-Phase Steels," *Metallurgical and Materials Transactions A*, vol. 30, no. 5, pp. 1193-1202, 1999.
- [52] E. O. Hall, "The Deformation and Ageing of Mild Steel: III Discussion of Results," *Proceedings of the Physical Society. Section B*, vol. 64, no. 9, pp. 747-753, 1951.
- [53] N. J. Petch, "The Cleavage Strength of Polycrystals," *Journal of the Iron and Steel Institute*, vol. 174, pp. 25-28, 1953.
- [54] N. Hansen, "Hall–Petch Relation and Boundary Strengthening," *Scripta Materialia*, vol. 51, pp. 801-806, 2004.
- [55] H. S. Kim and Y. S. Lee, "Size Dependence of Flow Stress and Plastic Behavior in Microforming of Polycrystalline Metallic Materials," *Proceedings of the Institution of Mechanical Engineers, Part C: Journal of Mechanical Engineering Science*, vol. 226, pp. 403-412, 2012.

- [56] D. Canadinc, H. J. Maier, P. Gabor and J. May, "On the cyclic deformation response of ultrafine-grained Al–Mg alloys at elevated temperatures," *Materials Science and Engineering A*, vol. 496, no. 1-2, pp. 114-120, 25 November 2008.
- [57] M. A. Meyers and K. K. Chawla, *Mechanical Metallurgy Principles and Applications*, Englewood Cliffs, New Jersey: Prentice-Hall, Inc., 1984.
- [58] T. Gladman, "Precipitation Hardening in Metals," *Materials Science and Technology*, vol. 15, pp. 30-36, 1999.
- [59] E. Orowan, *Internal Stress in Metals and Alloys*, London: The Institute of Metals, 1948, p. 451.
- [60] M. F. Ashby, *Oxide Dispersion Strengthening*, New York: Gordon and Breach, 1958, p. 143.
- [61] R. R. Ambriz and D. Jaramillo, "Mechanical Behavior of Precipitation Hardened Aluminum Alloys Welds," in *Light Metal Alloys Applications*, InTech, 2014.
- [62] M. Davis and N. Thompson, "Creep in a Precipitation-Hardened Alloy," *Proceedings of the Physical Society. Section B*, vol. 63, no. 11, pp. 847-860, 1950.
- [63] M. A. Asadabad, M. Goodarzi and S. Kheirandish, "Kinetics of Austenite Formation in Dual Phase," *ISIJ International*, vol. 48, no. 9, pp. 1251-1255, 2008.
- [64] G. R. Speich, V. A. Demarest and R. L. Miller, "Formation of Austenite During Intercritical Annealing of Dual-Phase Steels," *Metallurgical Transactions A*, vol. 12, no. 8, pp. 1419-1428, 1981.
- [65] C. I. Garcia and A. J. DeArdo, "Formation of Austenite in 1.5 Pct Mn Steels," *Metallurgical and Materials Transactions A*, vol. 12, no. 3, pp. 521-530, 1981.
- [66] J. Mahieu, B. C. De Cooman and J. Maki, "Phase Transformation and Mechanical Properties of Si-Free CMnAl Transformation-Induced Plasticity-Aided Steel," *Metallurgical and Materials Transactions A*, vol. 33, no. 8, pp. 2573-2580, 2002.
- [67] R. Neugebauer, A. Sterzing and M. Bergmann, "Mechanical properties of the AlSi1MgMn aluminium alloy (AA6082) processed by gradient rolling," *Materialwissenschaft Und Werkstofftechnik*, vol. 42, no. 7, pp. 593-598, 2011.
- [68] ASTM, "E8 Standard Test Methods of Tension Testing of Metallic Materials," in *Annual Book of ASTM Standards*, American Society for Testing and Materials, vol. 3.01.

- [69] P. A. Soloshi, N. J. Thimons, A. A. Marks, J. Hartle, Q. Trest, J. Adam, W. Perisse and A. J. DeArdo, "Sheared-Edge Ductility/ Hole-Expansion Ratio Testing of Advanced High-Strength Steels," in Materials Science and Technology (MS&T) 2015, Columbus, 2015.
- [70] L. Zhao, N. H. van Dijk, E. Bruck, J. Sietsma and S. van der Zwaag, "Magnetic and X-Ray Diffraction Measurements for the Determination of Retained Austenite in TRIP Steels," Materials Science and Engineering A, vol. 313, pp. 145-152, 2001.
- [71] R. W. Cahn and P. Haasen, Physical Metallurgy, 4th Edition, North Holland, 1996.
- [72] K. Hasegawa, K. Kawamura, T. Urabe and Y. Hosoya, "Effects of Microstructure on Stretch-flange-formability of 980 MPa Grade Cold-rolled Ultra High Strength Steel Sheets," ISIJ International, vol. 44, no. 3, pp. 603-609, 2004.
- [73] J. Chiang, B. Lawrence, J. D. Boyd and A. K. Pilkey, "Effect of Microstructure on Retained Austenite Stability and Work Hardening of TRIP Steels," Materials Science and Engineering A, vol. 528, no. 13, pp. 4516-4521, 2011.